

This is an earlier version of “Lu, Q. L., Sun, W., Dai, J., Schmöcker, J. D., & Antoniou, C. (2024). Traffic resilience quantification based on macroscopic fundamental diagrams and analysis using topological attributes. *Reliability Engineering & System Safety*, 110095. DOI: [10.1016/j.ress.2024.110095](https://doi.org/10.1016/j.ress.2024.110095)”.

---

# Traffic resilience quantification based on macroscopic fundamental diagrams and analysis using topological attributes

Qing-Long Lu<sup>a</sup>, Wenzhe Sun<sup>b</sup>, Jiannan Dai<sup>b</sup>, Jan-Dirk Schmöcker<sup>b</sup>, Constantinos Antoniou<sup>a</sup>

<sup>a</sup>Chair of Transportation Systems Engineering, Technical University of Munich, Germany

<sup>b</sup>Department of Urban Management, Kyoto University, Japan

## ARTICLE INFO

### 10 Keywords:

Traffic resilience  
Macroscopic fundamental diagram  
Infrastructure disruption  
Traffic simulation  
Network topology

15

20

25

## 1. Introduction

Transportation system disruption is defined as the state in which the system is not operating with its optimal efficiency. It can be caused by either demand-side factors such as daily recurring congestion and sudden demand peaks due to large events or emergencies, or supply-side factors such as infrastructure damage due to natural disasters (e.g., 30 earthquakes and hurricanes) or temporary link closures for planned events (e.g., marathons and concerts). Transportation system disruptions can cause significant losses in the urban economy and society as a consequence of the impairment of traffic efficiency (Kurth et al., 2020; Chacon-Hurtado et al., 2020; Chalkiadakis et al., 2022; Arango et al., 2023). To effectively respond to system disruptions, it is crucial to understand the system's reliability and functionality beforehand. The concept of *resilience* is established for this purpose. As an example, a conference series, 35 International Symposium on Transport Network Resilience (INSTR)<sup>1</sup>, has been devoted to the topic of transportation network resilience since 2001.

The U.S. Federal Highway Administration (FHWA) defines resilience in transportation systems as “*the ability to prepare for changing conditions and withstand, respond to, and recover rapidly from disruptions*” (FHWA, 2015). Mathematically, system resilience can be evaluated by integrating the deviation of system functionality from its optimal 40 state throughout the disruption period (Bruneau et al., 2003). Clearly, a reliable indicator of system functionality is critical to the evaluation of system resilience. Although the resilience concept has been adapted to transportation systems for more than two decades, there is no universally accepted definition of system functionality in the context of urban road transportation yet. Yang et al. (2023) summarized that 48 transport resilience indicators have been proposed in the literature. By convention, topological measures based on complex network theory, which can represent 45 the structural properties (e.g., connectivity and accessibility) of the network, are used (see Pan et al., 2021, for a review). Although some have extended these indicators by introducing stochastic simulation to provide a probabilistic evaluation, such as the eccentricity and heterogeneity measures proposed in Guidotti et al. (2017), traffic dynamics are

<sup>1</sup>✉ qinglong.lu@tum.de (Q. Lu); wz.sun@trans.kuciv.kyoto-u.ac.jp (W. Sun); dai@trans.kuciv.kyoto-u.ac.jp (J. Dai); schmoecker@trans.kuciv.kyoto-u.ac.jp (J. Schmöcker); c.antoniou@tum.de (C. Antoniou)

ORCID(s): 0000-0002-6087-8670 (Q. Lu); 0000-0002-7305-8671 (W. Sun); 0000-0002-4186-0088 (J. Dai); 0000-0003-2219-9447 (J. Schmöcker); 0000-0003-0203-9542 (C. Antoniou)

<sup>1</sup><https://instr.org>

## ABSTRACT

Transportation system disruptions significantly impair transportation efficiency. This paper proposes new indicators derived from the Macroscopic Fundamental Diagram (MFD) dynamics before and after a disruption to evaluate its impact on traffic resilience. Considering that MFD is an intrinsic property of a homogeneously congested transportation network, the resilience losses due to congestion and network disruption are measured separately. The resilience loss is defined as the reduction in trip completion rate, comparing congested cases to uncongested cases or disrupted cases to undisrupted cases. The resilience loss hence also exists for an undisrupted network and is measurable by the proposed method. A Simulation of Urban MObility (SUMO) model is calibrated by real origin-destination patterns, to allow for experiments in scenarios of different demand variations and supply disruptions. Case studies are conducted in Munich, Germany and Kyoto, Japan to test the usefulness of the newly proposed indicators. We furthermore explore the relationship between resilience loss and network topological attributes such as centrality and connectivity from a variety of synthetic disruption experiments in Munich and Kyoto. We find that the resilience loss in a grid-like network as in Kyoto is less dependent on the degradation of network connectivity than in a ring-like network as in Munich.

typically not considered in their applications. On the other hand, trip-based indicators, such as network average travel time (Dingil et al., 2019; Arango et al., 2023), average speed (Hoogendoorn et al., 2015), and demand served (Chen and Miller-Hooks, 2012), have also been adopted to overcome the drawbacks of the topology-based ones. However, these indicators based on direct trip information are usually sensitive to travel demand levels and patterns, and cannot be regarded as a property of the transportation system.

With the definition of the macroscopic fundamental diagram (MFD) (Geroliminis and Daganzo, 2008) and the success of its applications to perimeter control (e.g., Zhong et al., 2018; Chen et al., 2022), one can construct reliable and representative traffic resilience indicators by relating the MFD dynamics and system functionality. The MFD describes the relationship among the space-mean production, the space mean state, and spatial homogeneity in traffic flow, which provides a way to evaluate network performance without requiring detailed traffic physics. More importantly, MFD is an intrinsic property of a homogeneously congested transportation network (Huang et al., 2020; Su et al., 2020). Therefore, compared to the other measures, it holds the superiority of integrating information on transportation network characteristics, traffic dynamics, and travel demand patterns. Note that, essentially, transportation system disruptions always render recurring or non-recurring congestion. This provides an opportunity for measuring system resilience by comparing the MFD dynamics before and after disruptions. To date, several MFD-based resilience indicators have been proposed, including the link criticality index based on the shape of MFDs (Kim and Yeo, 2017), the performance indicator based on travel production (Amini et al., 2018), and the traffic resilience index based on total congestion deviation (Gao et al., 2022).

As a step in that direction, we present enhanced MFD-based traffic resilience indicators in this paper to address the defects in its predecessors. To be specific, we theoretically discuss and compare the influencing mechanisms behind hyper-congestion and supply-side disruptions, which are the transportation disruption cases mostly discussed in the literature (e.g., Gao et al., 2022; Zhang et al., 2022a; Pei et al., 2024), highlighting the need to differentiate the calculation of traffic resilience based on the type of disruption given their difference in the MFD dynamics changing patterns. Furthermore, to explore and evaluate the extent to which static topology-based resilience indicators can explain traffic resilience, we conduct a regression analysis on their relationship with the traffic resilience loss computed using the proposed indicators. To this end, this paper also describes the development of a common simulation-based scenario generation framework to test traffic resilience loss and derive topological attributes. To illustrate the applicability of our approach, we conduct case studies on two real networks, Munich, Germany, and Kyoto, Japan.

This paper contributes to the existing body of knowledge on traffic resilience and its practical implementation from the following perspectives. (i) We develop novel resilience indicators for transportation systems, emphasizing their function in serving traffic flows, leveraging the well-established MFD concept. Understanding the system functionality in the face of disruptive events is also an important topic within the realm of system reliability engineering. (ii) We build a regression model to describe the relationship between topological attributes of transportation networks and the traffic resilience of transportation systems. With this regression model, traffic resilience can be predicted solely based on the network structure, eliminating the necessity for detailed traffic flow information.

The rest of the paper is structured as follows. Section 2 reviews the related literature and identifies the literature gap. Section 3 presents the MFD-based traffic resilience indicators and discusses the necessity of distinguishing between hyper-congestion and supply-side disruptions. Section 4 describes the simulation-based scenario generation framework together with the regression model. Then, Section 5 introduces the network models of case studies and experiment scenarios. In Section 6, experiment results are analyzed and discussed. Finally, Section 7 concludes the paper with the findings of the research alongside future directions for research.

## 2. Related Literature

In this section, we conduct a comprehensive review of network-wide resilience indicators proposed for transportation systems/networks. In particular, we focus on two main categories: those based on simulation-based approaches and those developed using the concept of MFD. Besides, it is beneficial to discuss existing studies in the evaluation and optimization for urban transportation systems, as these serve as motivation for proposing resilience indicators. To gather relevant literature, we conducted a systematic search in the Scopus database. We retrieved and selected related publications using keyword combinations of “transportation network & resilience”, “resilience & traffic simulation”, and “resilience & macroscopic fundamental diagram” utilizing the tool developed by Narayanan and Antoniou (2022).

## 2.1. Transportation system resilience assessment

Existing studies on transportation system resilience exhibit variations in resilience definitions, indicators, and assessment methods, due to differences in the nature, scale, and impact of disruptions (Serdar et al., 2022). Resilience indicators, among others, are utilized in evaluating functionality in response to disruptions and guiding the enhancement of system infrastructure and components. Transportation networks, a typical type of multi-stage network, can attain more flexibility and efficiency in recovery strategies through resilience-based methods compared to distance-based and reliability-based methods (Liu et al., 2022, 2024). Here, the main disruption categories investigated and the approaches categories adopted are reviewed.

In the reviewed literature, seismic resilience and flood resilience are primary focuses due to the severe consequences of earthquakes and floods. Studies on seismic resilience primarily focus on post-earthquake recovery optimization. Given the role that bridges play in the resilience of road–bridge transportation networks, scheduling the recovery of bridges has been extensively studied. Various metrics have been utilized to determine bridge recovery schedules, including network connectivity and vehicular traffic (Ahmed et al., 2022), recovery time and cumulative benefit rate (Zhang et al., 2022a), network travel time (Zhang et al., 2022b), and recovery time and skewness of the recovery curve (Somy et al., 2022). There are also some studies that only performed pure assessment of resilience to seismic hazards. For instance, Virtucio et al. (2024) combines image-based bridge fragility generation and traffic simulations to assess earthquakes impacts on network resilience from an economic perspective. However, it is important to note that parallel restoration actions may cause unexpected downtime and impede network functionality recovery (Zhang et al., 2023c). Regarding flood resilience, various flood scenarios have been investigated, such as hurricane-induced flood (Dong et al., 2023), and precipitation-induced flood (Bucar and Hayeri, 2020; Wassmer et al., 2024). These investigations often rely on empirical analyses using historical data to evaluate the influence of floods on network topology, reliability, and stability (Dong et al., 2023; Bucar and Hayeri, 2020; Wassmer et al., 2024). Noteworthy, Zhang and Alipour (2023) proposed a two-stage stochastic programming approach to optimize pre-disruption mitigation and post-disruption recovery measures simultaneously to enhance resilience to flood hazards, where data-driven simulation was employed. However, in addition to seismic resilience and flood resilience, snow storm resilience and typhoon resilience have also received increasing attention in recent years, such as Mirjalili et al. (2023), Santiago-Iglesias et al. (2023), and Fang et al. (2022).

Some studies also explored resilience equality issues. For instance, Byun and D'Ayala (2022) provided a probabilistic analysis of disruption inequality across urban areas regarding seismic resilience. The inequality problem of disruptions has also been examined from the perspectives of socioeconomic groups and access to amenities (Wei et al., 2022; Anderson et al., 2022).

Evaluating the resilience of multi-modal transportation systems has emerged as a research hotspot in recent years, given the interdependence among different urban transportation systems such as subway, bus, and taxi. For instance, Wang et al. (2023) developed a dynamic resilience index that integrates passenger demand and infrastructure supply to assess the resilience of a multi-modal transportation system encompassing bus, subway, and taxi services. Chen et al. (2023) focused on the resilience of bus-metro interdependent networks, considering factors such as network topology damages and cascading failures when prioritizing nodes for recovery. Meanwhile, Zhang et al. (2023b) studied node reliability in multi-modal transportation networks, while Aparicio et al. (2022) conducted a comparative analysis of network metrics to evaluate the topological robustness of multi-modal transportation systems. Fang et al. (2022) proposed a multi-phase model to evaluate the resilience of complementary transportation systems of multiple modes in response to typhoon strikes. These studies collectively contribute to a deeper understanding of the resilience dynamics inherent in multi-modal transportation systems, thus providing valuable insights for enhancing their overall resilience in the face of disruptions.

Various models have been applied to address resilience-based evaluation and optimization problems, with notable categories including probabilistic models, mathematical optimization models, and data-driven models. Probabilistic models usually integrate a hazard component with a probability distribution of disturbance intensity, an evaluation component quantifying resilience, and a simulation component for mapping strategies to resilience outputs. For example, Amini and Padgett (2023) proposed a methodology integrating hazard and debris exposure models to assess the impact of hurricane-induced debris on transportation network resilience. Similar frameworks with probabilistic hazard modules, risk modules, and agent-based simulation modules were presented in Taghizadeh et al. (2023) and Wu and Chen (2023) to evaluate the seismic resilience of transportation systems during emergency medical responses. Additionally, Zhang et al. (2023a) applied a probabilistic recovery model to measure the restoration of bridges after earthquakes. In contrast, mathematical optimization models are applied to assist in planning pre-disruption mitigation

tion and post-disruption recovery strategies, subject to practical constraints such as budget, computational time, and personnel constraints (Serdar et al., 2022). Representative models include two-stage stochastic programming, where the first stage determines strategies while a number of disruption scenarios are simulated at the second stage (e.g., Zhang and Alipour, 2023), and bi-level optimization, where the upper-level model optimizes resource allocation and the lower-level model formulates user equilibrium (e.g., Amghar et al., 2024). However, these models often suffer from computational inefficiency, particularly in large-scale transportation networks. On the other hand, data-driven methods leverage sensor data, such as loop detector data and GPS data, collected over an extended period. With advancements in sensor technology and database storage and processing, these methods have also gained significant attention. Moreover, they hold promise for providing real-time information on resilience. For instance, Diab and Shalaby (2020) used metro system data to evaluate the impact of outdoor tracks and weather conditions on system resilience. Roy et al. (2019) proposed a method to detect disruptions from geo-located social media data and assess their impact on mobility resilience. A hybrid knowledge-based and data-driven approach was developed in Yin et al. (2022) with the aid of the Bayesian Network model and historical metro data to identify component weakness and enhance resilience with proper improvement. For a comprehensive review and comparison of these model categories, including their merits and limitations, readers are referred to Serdar et al. (2022).

In summary, while the aforementioned studies vary in terms of the disruptions of interest and the methods used for solution, they all rely on appropriate resilience indicators for evaluation and optimization purposes. Thus, there is a pressing need for a reliable resilience indicator to facilitate the application of the resilience concept in urban road transportation systems from the perspective of traffic flow.

## 2.2. Resilience indicators used in simulation-based evaluations

The evaluation of transportation network resilience has traditionally focused on purely topological measures derived from the theory of complex network analysis, such as connectivity (e.g., alpha index) and accessibility metrics (e.g., betweenness centrality) (see Table 1 in Zhang et al., 2015; Pan et al., 2021, for a review). While these static indicators provide some insight into the structural risk of transportation networks, they fail to characterize the impact of traffic demand changes and the development and cascading effects of disruptions in the spatial-temporal dimension (Shekar et al., 2017; Zeng et al., 2019; Xu and Chopra, 2022). In addition, these indicators also fail to evaluate the influence of a partial loss of capacity due to sub-links failure (there are usually multiple sub-links between two nodes in transportation networks) (Guidotti et al., 2017). To comprehensively assess the resilience of transportation networks, it is essential to incorporate traffic dynamics that capture the time-varying nature of network congestion.

In a comparative analysis conducted by Balal et al. (2019), multiple traffic dynamics-oriented resilience measures were examined, including queue length, link speed, link travel time, frontage road delay, and detour route delay. The study found a relatively low correlation among these measures, suggesting that the importance of links to network resilience depends on the specific measure employed. This finding implies that evaluating network resilience at the link level may lead to contradictory conclusions and offer limited contributions. Consequently, the need to reliably measure network performance in both spatial and temporal dimensions has pushed the evaluation of resilience beyond local traffic performance (e.g., travel time, speed, and delays of individual links or intersections) towards the development of network-wide measures (Miller-Hooks et al., 2012; Gao et al., 2016).

Bucar and Hayeri (2020) presented a framework for assessing the effects of precipitation-induced flood events in urban areas using a two-layer simulation model. Metrics such as vehicle miles traveled, vehicle hours traveled, and trips completed were employed to evaluate network resilience. Similarly, Hoogendoorn et al. (2015) evaluated network resilience by measuring changes in level-of-service due to density deviation caused by incidents. Average speed served as a proxy for level-of-service, making network resilience a function of density and density deviation. However, these indicators overlook the comparison between disruption and normal operation situations, as well as the time required for recovery, which are important considerations in defining resilience. Additionally, they make calculating the optimal system functionality (i.e., the equilibrium state before disruption) challenging, as they heavily depend on demand levels and patterns.

On the other hand, Chen and Miller-Hooks (2012) and Zhang et al. (2015) utilized the ratio of the maximum post-disaster throughput to the pre-disaster throughput as a resilience indicator. Chen and Miller-Hooks (2012) further employed this measure to optimize post-event recovery actions, while Zhang et al. (2015) used it to assess the significance of network topology in resilience. Yao and Chen (2023) applied the percolation theory, using the giant component size (i.e., the size of the largest connected component of the network), to evaluate network resilience to random failures. However, these indicators overlook traffic dynamics and their time-varying nature, thus providing an

inaccurate depiction of resilience along the temporal dimension.

### 2.3. Resilience indicators based on macroscopic fundamental diagram

In recent years, there has been significant interest among scholars in performance indicators based on the theory of the macroscopic fundamental diagram (MFD), since it represents an intrinsic property of a homogeneously congested transportation network. A brief introduction to the MFD is offered in Section 3.1. One of the pioneering efforts in this direction in the field of transportation resilience was made by [Kim and Yeo \(2017\)](#), who proposed a network performance loss indicator utilizing the concept of MFD to assess the criticality of network links. The indicator takes into account that disruptive events lead to increased spatial heterogeneity in traffic flow, thereby altering the shape of the MFD. The performance loss is quantified as the proportion of the aggregated flow reduction caused by disruptions, given by

$$FR = \frac{\int_{k_0}^{k_c} q(k) - q^d(k) dk}{\int_{k_0}^{k_c} q(k) dk} \quad (1)$$

where  $q(k)$  and  $q^d(k)$  are the weighted space-mean flow across the network under normal and disruption operation conditions, respectively;  $k_0$  and  $k_c$  represent the lower and upper bounds for comparison. However, in their definition,

- 5 both  $q(k)$  and  $q^d(k)$  are weighted based on the total length of the original network, without accounting for link removal during disruptions. This weighting scheme can lead to inaccurate comparisons ([Amini et al., 2018](#)). Furthermore, the comparison solely focuses on the shape of the MFD, disregarding the temporal dynamics of the network. Consequently, the comparison may introduce biases in cases where the MFD shape remains unchanged despite the occurrence of disruptive events, as will be demonstrated in the experiments conducted in Section 6.

To address these limitations, [Amini et al. \(2018\)](#) introduced an improved indicator by considering trip length changes in the evaluation of network resilience. They defined the service rate of a network as the number of completed trips per unit of time. Building upon the linear relationship discovered by [Geroliminis and Daganzo \(2008\)](#) between trip production ( $P$ ) and trip completion rate ( $D$ ), i.e.,  $P = \mathcal{L}D$ , where  $\mathcal{L}$  represents the average trip length, and leveraging the relationship between trip production and weighted flow, i.e.,  $P = \sum_{i \in \mathbb{L}} q_i l_i = qL$ , where  $L$  denotes the length of all links equipped with detectors, they derived a resilience index that reflects the network's service rate using weighted flow as a surrogate. The index is calculated as follows:

$$RI(t) = q(t) - q^d(t) \times \frac{\mathcal{L}}{\mathcal{L}_d} \quad (2)$$

- 10 where  $\mathcal{L}$  and  $\mathcal{L}_d$  are the average trip length under normal and disruption conditions, respectively. We note that this index has been normalized by  $L/\mathcal{L}$  without distinguishing the network before and after disruptions. It means, the same as in [Kim and Yeo \(2017\)](#), the length of the network is assumed unchanged during disruptions, which violates the reality of infrastructure disruptions.

Further, [Gao et al. \(2022\)](#) introduced a definition of traffic resilience for a system comprising two reservoirs, utilizing the total congestion deviation, which is measured as the difference between the operational vehicle accumulation and the optimal value. Assuming parabola-shaped MFDs, the traffic resilience is computed through the following equation:

$$TR = - \int_{t_0}^{t_c} \left| n_1(t) - \frac{n_1^{\max}}{2} \right| + \left| n_2(t) - \frac{n_2^{\max}}{2} \right| dt \quad (3)$$

where  $n_i(t)$  is the vehicle accumulation at reservoir  $i$  at time  $t$ , and  $n_i^{\max}$  is the corresponding maximum accumulation. The time interval from  $t_0$  to  $t_c$  represents the congestion period. A larger congestion deviation (the term inside the integral at a specific  $t$ ) represents severer congestion or more spare capacity. Note that this indicator is designed for evaluating the resilience to hyper-congestion. However, characterizing capacity spare as a measure of resilience loss may be unreasonable since it is primarily determined by limited travel demand rather than network malfunction. Resilience, as an indicator of system functionality, should not be affected by capacity spare. Additionally, using accumulation as a metric for transportation system performance, particularly during disruptions, has limitations. Firstly, the number of vehicles within the network, represented by accumulation, does not provide a comprehensive reflection

of transportation network functionality. The performance/functionality of a system/facility is generally represented by its service rate (i.e., the trip completion rate in MFD) rather than the number of customers (i.e., the accumulation in MFD). Secondly, the optimal accumulation during disruptions can exceed or equal that of normal operations, implying that the same accumulation value may result in lower resilience loss during disruptions, leading to inaccurate estimations.

**Table 1**

Notation

<b>Traffic resilience definition</b>	
$\Delta^d(t)$ [veh/h]	trip completion rate reduction at time $t$ due to congestion
$\Delta^s(t)$ [veh/h]	trip completion rate reduction at time $t$ due to supply-side disruptions
$R^d$ [veh]	resilience loss due to congestion
$R^s$ [veh]	resilience loss due to supply-side disruptions
$D(t)$ [veh/h]	trip completion rate at time $t$
$D_c$ [veh/h]	optimal trip completion rate
$k(t)$ [veh/km]	weighted space-mean density at time $t$
$k_c$ [veh/km]	critical weighted space-mean density
$q(t)$ [veh/h]	weighted space-mean flow at time $t$
$q_c$ [veh/h]	optimal weighted space-mean flow
$H(\cdot)$	Heaviside step function
$P(t)$ [veh]	trip production of the entire network at time $t$
$\mathbb{L}$	set of links in the directed network $G$
$\mathcal{L}$ [km]	average trip length
$L$ [km]	total length of all links of the network
$\gamma$	scaling factor between trip completion rate and weighted space-mean flow
<b>Synthetic scenario generation</b>	
$r$	random seed
$\mathbb{S}$	disruption scenario — a set of closed/damaged links
$G$	directed graph of the complete network
$G(\mathbb{S})$	directed graph of the disruptive network of scenario $\mathbb{S}$
$\mathbf{x}$	vector of topological attributes
$S$	traffic simulator
$M$	origin-destination demand matrix
$Y$	simulation outputs
$\theta$	vector of parameters of the regression model
$\rho$	hyper-parameter related to the $l_1$ -norm regularization term
$f(\mathbf{x}; \theta)$	linear model with explanatory variables $\mathbf{x}$ and parameters $\theta$

### 3. MFD-based traffic resilience to disruptions

In order to address the limitations of existing resilience indicators discussed in Section 2, we propose comprehensive MFD-based traffic resilience indicators in this section, partially building upon the work presented by Amini et al. (2018). Our approach acknowledges the need to differentiate between the evaluation of traffic resilience to hyper-congestion and supply-side disruptions due to the distinct mechanisms through which they exert influence on the system. This differentiation is crucial for devising and implementing appropriate preparedness and recovery strategies to mitigate their impact and enhance network resilience. In particular, hyper-congestion typically involves recurring events, allowing for the application of conventional network traffic optimization methods to improve resilience. On the other hand, supply-side disruptions are typically non-recurring events that require event-specific and tailored approaches. By distinguishing between these two types of disruptions, we can better understand the unique challenges they pose and identify the most effective response measures to enhance resilience. We introduce the notation listed in Table 1 for ease of explanation.

### 3.1. Introduction to the macroscopic fundamental diagram

The MFD describes the relationship between the number of vehicles on a network and their average speed. Essentially, it provides insights into the network's internal flow (represented by the number of vehicles per roadway length or weighted average density) and its outflow (represented by the trip completion rate or weighted space-mean flow).

- 5 Figure 1 illustrates the typical parabolic shape of an MFD. One of the key advantages of the MFD is its simplicity and applicability in real-time control problems, such as perimeter control, as it does not require extensive traffic data from multiple sources or complex estimation methods. The MFD can be constructed using raw field data obtained from common loop detectors or floating car data. Moreover, the MFD is an intrinsic property of a homogeneously congested transportation network and remains independent of traffic demand. This makes it a valuable tool for analyzing and optimizing transportation systems under varying conditions.
- 10

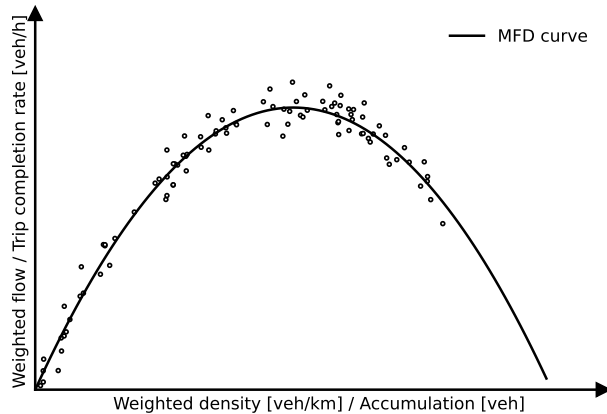


**Figure 1:** Macroscopic fundamental diagram (MFD).

Specifically, for a certain time step, the weighted average density and the weighted space-mean flow are given by

$$k(t) = \frac{\sum_{i \in \mathbb{L}} l_i k_i(t)}{\sum_{i \in \mathbb{L}} l_i} \quad (4)$$

$$q(t) = \frac{\sum_{i \in \mathbb{L}} l_i q_i(t)}{\sum_{i \in \mathbb{L}} l_i} \quad (5)$$

where  $\mathbb{L}$  is the set of links with loop detectors installed,  $l_i$  presents the length of link  $i$ ,  $k_i$  and  $q_i$  represents the vehicle density and flow at link  $i$ , respectively. Meanwhile, accumulation is the total number of vehicles in the network, which is usually difficult to acquire in practice. Nonetheless, since the roadway length is fixed, the accumulation is proportional to the density. It can be estimated as

$$\hat{n}(t) = \sum_{i \in \mathbb{L}} l_i k_i(t) \quad (6)$$

where  $n$  represents accumulation.

Similarly, directly measuring the trip completion rate is often challenging. Therefore, it becomes necessary to estimate it using readily available traffic variables that can be easily estimated. A notable finding by [Geroliminis and Daganzo \(2008\)](#) is that the trip completion rate exhibits a linear relationship with the trip production, with the average vehicular trip length serving as a scaling factor. Thus, we can estimate it as

$$D(t) = P(t)/\mathcal{L} \quad (7)$$

where  $D(t)$  denotes the trip completion rate,  $P(t)$  denotes the network trip production,  $\mathcal{L}$  denotes the average trip length. To estimate  $P(t)$ , we can utilize the product of the network length and the weighted space-mean flow, denoted as  $\hat{P}(t) = Lq(t)$ . Therefore, we can estimate the trip completion rate as below.

$$\hat{D}(t) = \frac{q(t)}{\gamma} \quad (8)$$

where  $\gamma = \mathcal{L}/L$  denotes a scaling factor.

### 3.2. Traffic resilience to congestion

As per the definition of transportation system resilience proposed by FHWA (FHWA, 2015), we define traffic resilience as below.

- 5 **Definition 1** (Traffic resilience). *Traffic resilience represents the ability of an urban road transportation system to prepare for different kinds of disruptions, effectively serve vehicles, and recover rapidly to its optimal serving rate (i.e., trip completion rate).*

Hyper-congestion, here refers to situations of congestion resulting from extremely high demand. To make it general, traffic resilience to congestion is discussed in this study. During such disruptions, the transportation network is unable

- 10 to serve users (vehicles) as efficiently as under normal operations due to the intricate interactions among vehicles in congested states and the propagation of traffic congestion. In essence, the resilience loss under congestion stems from the fact that it prevents the transportation network from operating at its optimal performance level, which is indicated by the states in the MFD where vehicle accumulation exceeds its critical value.

Considering that the primary function of transportation networks is to facilitate the mobility of people and goods (Jana et al., 2023), the trip completion rate (measured in vehicles per hour) represents the network's service rate. Hence, the performance loss under congestion can be evaluated by quantifying the reduction in trip completions. Specifically, for a given time  $t$ , the reduction in trip completions can be calculated by

$$\Delta^d(t) = (D_c - D(t)) H(k(t) - k_c) \quad (9)$$

where  $\Delta^d(t)$  represents the trip completion reduction,  $D_c$  is the optimal trip completion rate identified using MFD. The superscript  $d$  in  $\Delta^d(t)$  refers to demand-side disruptions (here, congestion), which is used to distinguish from supply-side disruptions introduced in Section 3.3.  $k(t)$  is the weighted average density at time  $t$  given by  $k(t) = \sum_{i \in \mathbb{L}} l_i k_i(t) / \sum_{i \in \mathbb{L}} l_i$  where  $\mathbb{L}$  is the set of links equipped with detectors, and  $k_c$  is the critical density.  $H(k(t) - k_c)$  is an indicator function (here, a Heaviside step function) defined as

$$H(k(t) - k_c) := \begin{cases} 1 & k(t) - k_c \geq 0 \\ 0 & k(t) - k_c < 0 \end{cases} \quad (10)$$

This function effectively eliminates the consideration of capacity spare in the evaluation.

Then, the resilience loss can be quantified by the integral of trip completion reduction along the disruption period.

$$R^d = - \int_{t_0^d}^{t^d} \Delta^d(t) dt = - \int_{t_0^d}^{t^d} (D_c - D(t)) H(k(t) - k_c) dt \quad (11)$$

- 15 where the time from  $t_0^d$  to  $t^d$  indicates the congestion period or the time period of interest.

Hence, given  $\hat{D}_c = q_c/\gamma$ , substituting Equation (8) into Equation (11), the resilience loss can be estimated by

$$\hat{R}^d = - \int_{t_0^d}^{t^d} \left( \frac{q_c}{\gamma} - \frac{q(t)}{\gamma} \right) H(k(t) - k_c) dt \quad (12)$$

By utilizing Equation (12) with a specified  $\gamma$  value, we can compute the traffic resilience loss of the network contributed by congestion solely using loop detector data. The parameter  $\gamma$  can be estimated by utilizing floating car data or simulation data generated from the corresponding calibrated simulation model.

### 3.3. Traffic resilience to supply-side disruptions

- 20 Supply-side disruptions refer to modifications to the network structure, such as temporary closures of links, intersections, or regions due to specific events (e.g., marathons, concerts), infrastructure malfunctions caused by natural or man-made disasters (e.g., earthquakes, cyberattacks).

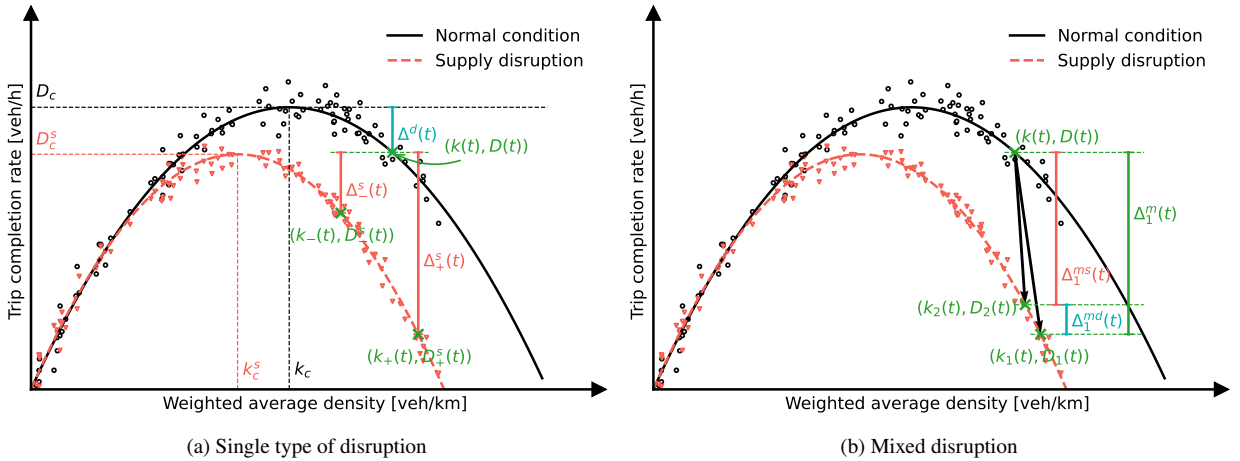


**Figure 2:** Graphical illustration of the definition of traffic resilience to disruptions.

Unlike demand-side disruptions, supply-side ones result in resilience loss by affecting the shape of the MFD. Generally, a “shrinkage” of the MFD is anticipated. Figure 2a illustrates an instance where the MFD under supply-side disruptions is situated below the MFD under normal operational conditions. However, it is crucial to note that this example may not accurately represent all transportation networks. In some cities, for instance, the condition  $k_c^s < k_c$  5 may not hold, as we will demonstrate in Section 6. Similarly, the critical accumulation may not always be smaller under supply-side disruptions.

The resilience of a transportation system under supply disruptions can be measured by comparing the dynamics of the MFD before and after the disruption. Note, the resilience loss caused by congestion under normal conditions should be removed from the calculation of the resilience loss induced by supply-side disruptions. The difference between the distances of the optimal trip completion rate to the completion rate under normal conditions and to the value under disruption conditions is employed to quantify the resilience loss solely attributable to supply disruptions. Mathematically, the trip completion reduction caused by supply disruptions, denoted as  $\Delta^s$ , is calculated as follows:

$$\Delta^s(t) = \max \{ (D_c - D^s(t)) - (D_c - D(t)), 0 \} = \max \{ D(t) - D^s(t), 0 \} \quad (13)$$

While  $(D_c - D^s(t))$  computes the total reduced trip completion rate under the supply-side disruption,  $(D_c - D(t))$  computes the reduced trip completion rate due to traffic congestion if there is no supply-side disruption. Then, their difference gives the reduced trip completion rate solely caused by the supply disruption.

10 The density under disruptions is usually not equal to what it should be under normal situations. For instance, as depicted in Figure 2a, assume the traffic state without disruptions is represented by  $(k(t), D(t))$  at time  $t$ . Under disruptions, it can be characterized by  $(k_-(t), D_-(t))$  or  $(k_+(t), D_+(t))$ , indicating that the density may be lower or higher. Nonetheless, it is intuitive to expect that traffic will become denser (the latter case) if the demand is not changed as the number of available links within the network decreases. However, in practice, some travelers might cancel their trips, leading to the former case.

15 Then, the resilience loss due to supply-side disruptions can be quantified by the integral of trip completion reductions along the disruption period.

$$R^s = - \int_{t_0^s}^{t^s} \Delta^s(t) dt = - \int_{t_0^s}^{t^s} \max \{ D(t) - D^s(t), 0 \} dt \quad (14)$$

where the time from  $t_0^s$  to  $t^s$  indicates the disruption period or the time period of interest.

Similarly, given the linear relation between the trip completion rate and the weighted space-mean flow (i.e.,  $\hat{D}(t) = Lq(t)/\mathcal{L} = q(t)/\gamma$ ), we can estimate the resilience loss caused by supply-side disruptions by

$$\hat{R}^s = - \int_{t_0^s}^{t^s} \max \left\{ \frac{q^s(t)}{\gamma^s} - \frac{q(t)}{\gamma}, 0 \right\} dt \quad (15)$$

Where  $\gamma^s = \mathcal{L}^s/L^s$ . We distinguish  $\gamma$  and  $\gamma^s$  here because the average trip length and the length of the available network are different under normal conditions and under supply-side disruptions due to rerouting and link closures.

### 3.4. Traffic resilience to coupling of supply disruptions and increased demand

While we have discussed the situations of demand reduction and demand unchanged under supply-side disruptions,

- 5 it is often the case that sudden supply disruptions trigger demand surges. For example, emergency demand or evacuations can lead to a sudden demand increase ([Safitri and Chikaraishi, 2022](#)). This leads to a mixed disruption scenario combining supply disruptions with increased demand, which would result in more severe congestion and further impact traffic resilience.

Figure 2b illustrates a possible situation of a mixed disruption scenario. Assume the traffic state under normal conditions is at  $(k(t), D(t))$ . With the occurrence of a supply disruption, the traffic state changes to  $(k_1(t), D_1(t))$ . In this case, the change is attributed to both the supply disruption and the emergency demand increase. Therefore, the traffic resilience loss calculated using Equation (15) reflects the combined impact of both factors, denoted as  $\Delta_1^m(t)$ . Assuming a disruptive traffic state without the surge in demand is represented by  $(k_2(t), D_2(t))$ , the traffic resilience loss solely due to the supply disruption ( $\Delta_1^{ms}(t)$ ) is smaller than  $\Delta_1^m(t)$ . The difference between them is the portion attributed to congestion induced by the emergency demand, denoted as  $\Delta_1^{md}(t)$ .

In practice, leveraging Equation (15), we can obtain  $\Delta_1^m(t)$  and  $\Delta_1^{ms}(t)$  by running simulations with augmented demand and normal demand, respectively. Then, the loss due to demand increase can be estimated as  $\Delta_1^{md}(t) = \Delta_1^m(t) - \Delta_1^{ms}(t)$ . Noteworthy is that, in addition to the difference in demand, the scaling factors ( $\gamma^s$ ) for  $\Delta_1^m(t)$  and  $\Delta_1^{ms}(t)$  may also differ due to vehicle rerouting and detouring.

### 20 3.5. Physical interpretation of traffic resilience

As per the proposed definition of traffic resilience (Definition 1) and corresponding formulations, physically, traffic resilience loss due to congestion  $R^d$  [veh] and supply-side disruptions  $R^s$  [veh] represent the cumulative number of vehicles that should have finished their trips within the respective planned time intervals under optimal operational conditions and in the absence of any supply disruptions, respectively.

25 Figure 3 provides an illustrative example showcasing the change of trip completion rates under normal conditions and supply-side disruptions from 6 am to 8 pm. It visualizes the corresponding traffic resilience losses. In this example, two demand peaks are observed at 8 am (morning peak) and 5 pm (evening peak). Within the congestion period from  $t_0^d$  to  $t^d$  (assuming that the system returns to be uncongested at  $t^d$ ), the traffic resilience loss due to congestion is measured by the area between  $D_c$  and the curve of  $D(t)$ . Conversely, the traffic resilience loss due to supply-side disruptions is measured by the area between  $D(t)$  and  $D^s(t)$  when  $D(t) > D^s(t)$ . When the demand reduces to a certain level (below the service rate under supply-side disruptions),  $D^s(t)$  will exceed  $D(t)$ . In this case, the system is serving the “cumulative vehicles” that were delayed by the disruption. We refer to these delayed vehicles as the network queue, as indicated in Figure 3. In other words, the network queue ([veh]) at time  $t$  is the remaining portion of traffic resilience loss ([veh]) that has not been served.

### 35 3.6. Normalization and discretization

Comparing the resilience of transportation networks across different cities has been a longstanding interest within the transportation community (e.g., [Ganin et al., 2019](#); [Kurth et al., 2020](#); [Yin et al., 2023](#)). However, such comparisons require normalization due to the inherent differences in city scales, including factors such as area, population, and car ownership. To address this, we utilize the optimal trip completion rate, which defines the optimal functionality of the system, as a normalization factor for the trip completion reductions. This allows us to calculate the normalized resilience losses, which are given by

$$\tilde{R}^d = - \int_{t_0^d}^{t^d} \left( \frac{D_c}{D_c} - \frac{D(t)}{D_c} \right) H(k(t) - k_c) dt = - \int_{t_0^d}^{t^d} \left( 1 - \frac{q(t)}{q_c} \right) H(k(t) - k_c) dt \quad (16)$$

$$\tilde{R}^s = - \int_{t_0^s}^{t^s} \max \left\{ \frac{D(t)}{D_c} - \frac{D^s(t)}{D_c}, 0 \right\} dt = - \int_{t_0^s}^{t^s} \max \left\{ \frac{q(t)}{q_c} - \frac{\gamma q^s(t)}{\gamma^s q_c}, 0 \right\} dt \quad (17)$$

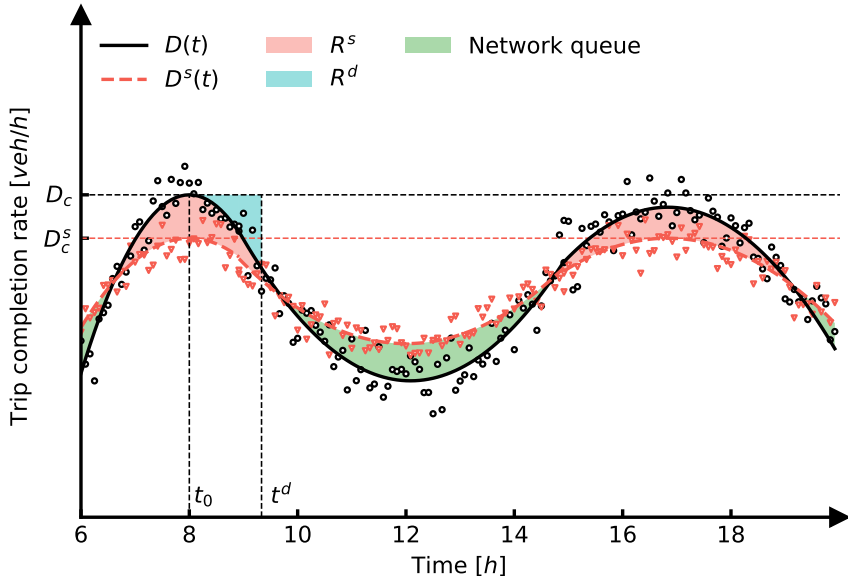


**Figure 3:** Graphical illustration of the calculation of traffic resilience.

Similarly, the normalized traffic resilience losses  $\tilde{R}^d$  and  $\tilde{R}^s$  can be interpreted as the cumulative percentage of service rate impairment resulting from suboptimal operational states caused by congestion and supply-side disruptions, respectively.

The traffic resilience formulations discussed above are derived for continuous observations. However, in practice, traffic dynamics are collected and aggregated into discrete time intervals. In this case, we can calculate the trip completion reduction within each time interval and then estimate the total traffic resilience losses by summing up the reductions over all intervals. The estimation of total traffic resilience losses in discrete time intervals can be expressed as follows:

$$\hat{R}^e = -\frac{T}{2} \sum_{t=1}^{N_t} (\hat{\Delta}^e(t) + \hat{\Delta}^e(t-1)) \quad (18)$$

where  $e \in [d, s]$  indicates the type of disruption events,  $T$  is the length of time intervals (assuming all time intervals share the same length), and  $N_t$  is the total number of time intervals within the period of interest. We assume that the period of interest starts before the disruption events, such that we have  $\hat{\Delta}^e(0) = 0$ .

#### 4. Regression model of the relationship of traffic resilience with network topology

Topological attributes play a critical role in the resilience property of transportation networks (Zhang et al., 2015; Pan et al., 2021; Hao et al., 2023). For instance, attributes such as the Alpha index and betweenness centrality can effectively characterize the connectivity and accessibility of the corresponding network, respectively. It follows that they have been extensively employed to define and assess transportation system resilience. However, those metrics fail to capture the traffic dynamics of the system, and applying a single metric of them to evaluate urban transportation systems may lead to unreliable conclusions. To address this limitation, some studies (such as Levinson, 2012; Parthasarathi, 2014; Huang and Levinson, 2015; Kurth et al., 2020; Wang et al., 2023; Yin et al., 2023) have been proposed to model the relationship between topological attributes and traffic dynamics so as to understand to which extent network topology can determine the operation of the associated transportation system. However, all of them have at least one of the following limitations: (i) Different transportation networks are included in a single model regardless of the topology type/style (e.g., grid-like, scale-free); (ii) The influence of demand level on the dependent variable is overlooked. Regarding the first limitation, the experiment results presented in Section 6 will show that the relationship model varies among different topology types.

In this study, we are interested in the relationship between topological attributes and traffic resilience under supply-side disruptions defined in Section 3. The reason why congestion is not included is that it often refers to recurring events, while supply-side disruptions pertain to non-recurring events. Also, only the latter events will change the network topology. To model the relationship, observations recording the network structure and traffic states under different disruptive events are required. However, given the rarity of such events, it is nontrivial to collect sufficient data. Traffic simulation provides an economic and reliable way to address this problem. In this section, we propose a systemic method to generate statistically significant samples by creating numerous synthetic supply disruptions for estimating the relationship model, which can also address the aforementioned limitations in previous studies.

Figure 4 demonstrates the process of creating a synthetic sample. The following description is dedicated to a certain city network (we denote its complete form by  $G$ ) and a certain demand matrix (denoted by  $M$ ).

- Step (1) The process starts with a certain percentage number  $p \in [0, 1]$ , indicating the percentage of links that are blocked or damaged due to the disruptive event.
- Step (2) With a certain random seed  $r$ , a disruption scenario  $\mathbb{S}$  is created, by randomly sampling the links to be closed. Essentially, a disruption scenario  $\mathbb{S}$  can be expressed as a set of closed links.
- Step (3) Relevant topological attributes  $\mathbf{x}$  describing the network topology are derived from the damaged network  $G(\mathbb{S})$ .
- Step (4) Run traffic simulations ( $\mathcal{S}$ ) using the damaged network  $G(\mathbb{S})$  and the demand matrix  $M$  to generate traffic dynamics  $Y(\mathbb{S})$ . Note that in order to obtain statistically significant results, multiple simulation replications are necessary for each disruption scenario. Furthermore, the portion of demand originating from or terminating at the closed links is removed during simulations, representing the canceled trips in reality.
- Step (5) From the traffic dynamics of all simulation replications, we can estimate the mean traffic resilience loss  $R^s(\mathbb{S})$ . Finally, the tuple  $(\mathbf{x}, R^s)$  constitutes a synthetic observation.

By repeating this process for different  $r$ 's under the same  $p$  and for different  $p$ 's, we can create a synthetic dataset  $(X, R)$  of disruption observations.

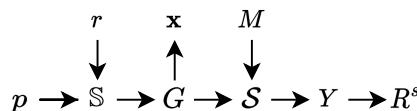


**Figure 4:** Graphical illustration of generating scenarios for regression analysis.

Table 2 lists some selected typical topological attributes that are commonly considered in complex network topology analysis together with the respective metrics (Hagberg et al., 2008; Zhang et al., 2015; Boeing, 2017). Note that while transportation networks are directed graphs, some metrics are defined for undirected graphs only. For calculating these metrics, the corresponding undirected graph of the network is used. The listed metrics can explain the properties of the network across multiple aspects and are used in the regression analysis in this study. Readers are referred to Boeing (2017) and Wang et al. (2023) for more details about these attributes and metrics.

Using the synthetic dataset, a regression model can be estimated to describe the relationship between topological attributes and traffic resilience loss for a certain type of network topology. Recall that traffic resilience loss is a relative value derived from the difference between the traffic dynamics under disruptive and normal operations. Consequently, in order to measure how the degree of resilience relates to the changes in topological attributes, the explanatory dataset  $X$  should also be normalized with the corresponding values of the complete networks and transformed into relative percentage values. Mathematically, for a variable  $X_i$ , it is transformed into

$$Z_i = \frac{X_i}{X_i^c} - 1 \quad (19)$$

where  $X_i^c$  is a scalar representing the  $i$ -th topological metrics computed from the complete network,  $Z_i$  represents the transformed variable of  $X_i$ . We emphasize that this transformation is necessary for obtaining better model interpretability, and this treatment also differs our model from the previous ones.

**Table 2**  
Typical topological attributes

Attribute	Metric	Description
Basic statistics		
Network statistics	Number of nodes Number of links Average node degree Total length of all edges Average length of all edges	
Directed graph		
Assortativity	Degree assortativity  Average neighbor degree	The assortativity coefficient is the Pearson correlation coefficient of degree between pairs of linked nodes. It indicates the similarity of connections with respect to node degree.  The average neighbor degree of a node measures the average degree of all nodes within the neighborhood of a specific node.
Centrality	Average degree centrality Load centrality Edge load centrality Harmonic centrality	The average of the fraction of nodes that a node is connected to. The average of the fraction of all shortest paths passing through a node. The average of the fraction of all shortest paths passing through an edge. The average of the sum of the reciprocal of the shortest path distances from all other nodes to a node.
Connectivity	Alpha index Beta index Gamma index	Ratio of existing circuits to the maximum possible circuits. Ratio between the number of links and number of nodes. Ratio of the number of links to the maximum possible number of links.
Reciprocity	Reciprocity	Ratio of the number of edges pointing in both directions to the total number of edges.
Undirected graph		
Clustering	Average clustering coefficient	The clustering of a node is the fraction of possible triangles through that node that exists. For a given node, a triangle is formed if it is connected to its two neighbors. The average clustering coefficient of a graph is then the mean of local clustering.
Efficiency	Global efficiency	The efficiency of a pair of nodes in a graph is the multiplicative inverse of the shortest path distance between the nodes. The average global efficiency of a graph is the average efficiency of all pairs of nodes.

Employ a regularized linear regression, we can estimate the parameters by least squares as below:

$$\theta^* = \operatorname{argmin}_{\theta} \sum_i (f(\mathbf{x}_i; \theta) - R_i^s)^2 + \rho |\theta|_1 \quad (20)$$

where  $\mathbf{x}_i$  denotes the  $i$ -th sample in  $X$  and  $R_i^s$  is the corresponding resilience loss,  $\theta$  denotes the vector of parameters to be estimated.  $f(x; \theta)$  is a linear function with respect to  $\theta$  and its specific form depends on the transportation network of interest and the variable selection procedure.  $|\theta|_1$  denotes the  $l_1$ -norm regularization of the coefficients. The  $l_1$ -norm term is also served as a built-in feature selection method, thereby leading to sparse solutions.  $\rho$  is a hyper-parameter, indicating the weight of the penalty term. Equation (20) represents a lasso model.

## 5. Experimental design

### 5.1. Study areas and simulation setup

To examine the proposed traffic resilience indicators and explore their correlation with topology-based indicators, we implement case studies in two cities of different types of road network topology/layout. Specifically, we selected the city center of Munich, Germany, which features a central ring network, and the city center of Kyoto, Japan, known for its typical grid network. Figure 5 provides the maps of the two study areas and the corresponding network structure. Residential links are excluded from both networks.

The concerning area of Munich is about  $10 \text{ km} \times 10 \text{ km}$  ( $100 \text{ km}^2$ ) large, covering the busiest streets and commercial areas in Munich. The network consists of 2605 links with 564 detectors. The Kyoto study area spans approximately  $6 \text{ km} \times 8 \text{ km}$  ( $48 \text{ km}^2$ ). The selected area covers the main city of Kyoto, enclosed by four main roads in different directions. The network consists of 1189 links with 217 detectors. In both networks, detectors are fairly evenly distributed, as shown in Figure 5.

Simulation of Urban MObility (SUMO, Lopez et al., 2018), an open-source traffic simulator, is used to generate traffic dynamics for estimating the MFDs under various scenarios that are expounded on in Section 5.2 and 5.3. All scenarios are simulated at the mesoscopic resolution with a non-iterative dynamic stochastic user assignment method that approximates the dynamic user equilibrium (DUE) (Lu et al., 2023). To reduce the influence of the stochasticity in simulations, results from 10 replications are used to analyze the MFD dynamics of each scenario and estimate relevant variables, such as the critical average density and the optimal weighted space-mean flow. For each scenario, the traffic between 6 am and 10 am are simulated, with the first and last half an hour as the simulation warm-up and dissipation periods, respectively. For ensuring reliable simulation results, we also conduct a calibration on the mesoscopic simulation models. For ease of reading, the calibration process is omitted here and is described in Appendix A.

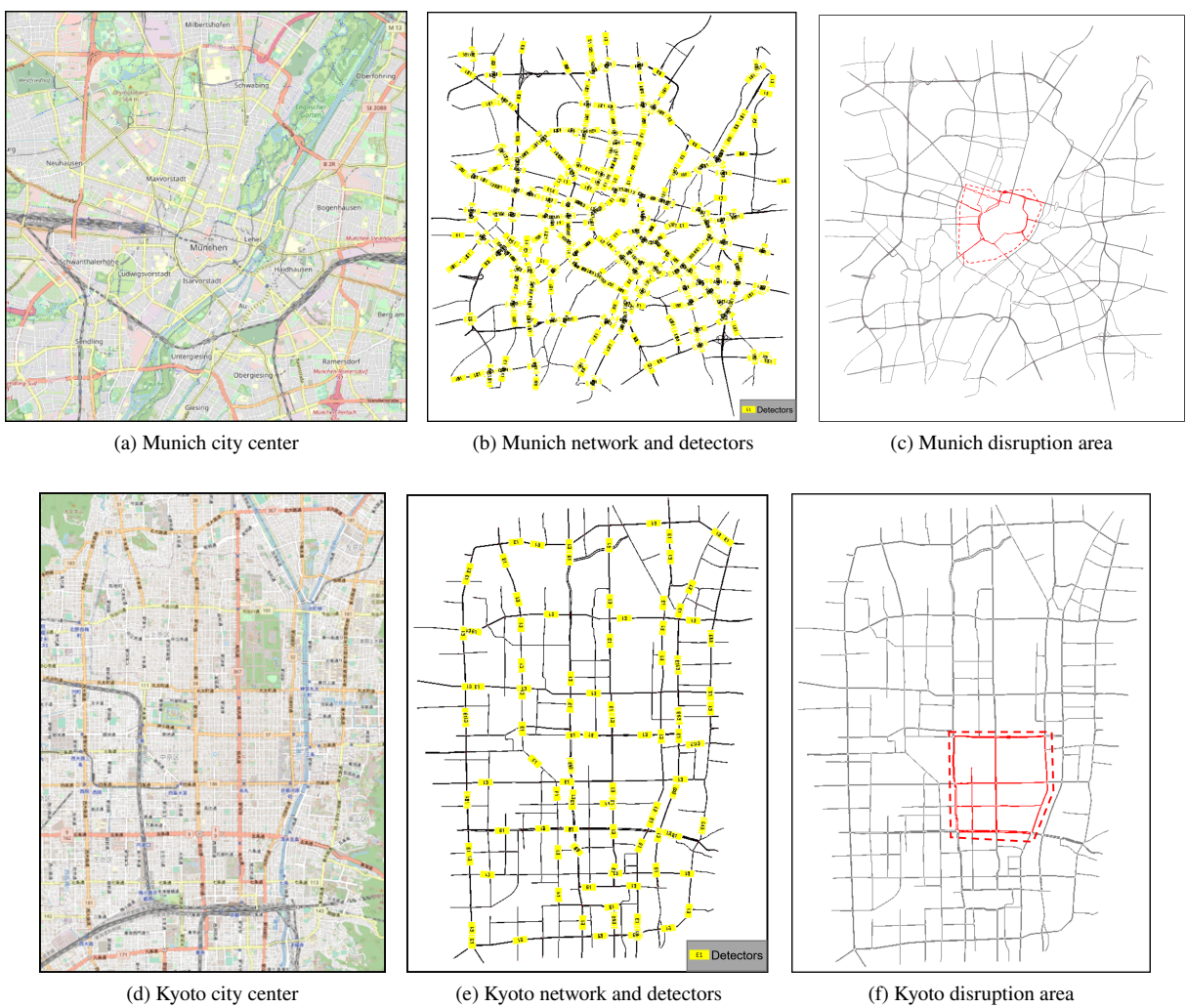


**Figure 5:** Study areas, networks and locations of detectors.

## 5.2. Demand variations and supply-side disruption scenarios

To demonstrate the MFD dynamics under different demand scenarios and to validate the underlying assumptions in the proposed approach, we consider three different travel demand levels: small demand (SD), medium demand (MD), and large demand (LD). The SD scenario represents the original demand level, while the MD and LD scenarios correspond to 1.2 and 1.5 times of the original demand, respectively. For each study area, all three demand scenarios are simulated.

At regular times of the year, various events are held in Kyoto, such as the Gion Festival<sup>2</sup> in July. During the Gion Festival, Shijo, the main road in the center of Kyoto, and the surrounding roads are temporarily controlled at night for about one to two weeks, during which motor vehicles are prohibited from entry. Figure 5f shows the area that might be closed temporarily during the festival. Temporary link/area closures due to such special events can render the supply-side disruptions (SSD) discussed in this study. Therefore, the SSD scenario of the Kyoto network is defined as the closure of links highlighted in Figure 5f from 7:00 to 8:00, during which 85 links (7% of all) are closed. All links are open outside this period. Due to a lack of required demand data, the closure is set in the morning rather than evening as in reality. However, this does not affect the validity of the conclusions drawn from the experimental results presented later in this paper. On the other hand, for comparative analysis, we create a similar SSD scenario in the Munich network. The area closure indicated in Figure 5c serves as the hypothetical SSD scenario. Similarly, 209 links (8% of all) are closed from 7:00 to 8:00. The two SSD scenarios result in comparable proportions, accounting for 7% and 8% of closed links in their respective networks. Notably, these closed links correspond to the busiest areas within the networks. This intentional design allows for a direct comparison of traffic resilience to supply disruptions between the two networks, which have different structural layouts.

## 5.3. Synthetic network disruption scenarios for regression

In order to understand the relationship between traffic resilience and topological attributes, we want to estimate a regression model between them with traffic resilience loss as the dependent variable. Unlike the previous studies incorporating transportation networks of different cities into a single model regardless of the type of topology, we acknowledge that their relationship may differ across topology types or cities, based on findings from case studies in Munich and Kyoto. Therefore, we adopt the scenario generation procedure proposed in Section 4 to generate numerous synthetic disruption scenarios for each city separately, leveraging the advance in traffic simulators and relevant interfaces.

More specifically, for each city, we consider a range of percentages from 2% to 20%, with a 2% interval, resulting in 10 different percentage values  $p$ . For each  $p$ , 100 disruption scenarios are constructed by randomly removing  $p$  percent of links from the complete network for each scenario. Finally, 1000 scenarios are constructed. It is worth mentioning that, isolated nodes will be removed from the network as well, if any, after removing a set of links. Vehicle trips without route connections, after the link removal, are considered as interrupted trips that will be explained more in Section 6.1. For each scenario, as described in Section 4, the topological attributes listed in Table 2 will be derived from the disruptive network, and the corresponding traffic resilience loss will be calculated using the traffic dynamics generated from SUMO. Note, here traffic dynamics only include the measurements collected by loop detectors, i.e., traffic flow, occupancy, and mean speed, to mimic real-world conditions. All traffic measurements are aggregated every five minutes. Furthermore, the scaling factor  $\gamma^s$  relating to the trip completion rate and weighted flow have to be distinguished among scenarios to ensure accurate comparisons.

## 6. Results

In this section, we first analyze the feasibility of using weighted space-mean flow as a proxy of trip completion rate and subsequently depict the dynamics of the MFD in the scenarios outlined in Section 5.2. Then, we evaluate the traffic resilience loss in those scenarios and conduct a comparative analysis between the Munich network and Kyoto network. Lastly, we explain the relationship between traffic resilience and topology-based indicators.

### 6.1. Trip completion rate estimation using a proxy

As the trip completion rate cannot be directly calculated from loop detector data, we utilized the production per unit length (weighted space-mean flow) as a proxy, leveraging the linear relationship between them. Considering the changes in the average trip length and the total length of the network under supply-side disruptions, the linear

<sup>2</sup>See <https://www.yasaka-jinja.or.jp/event/gion/> for more information about the festival.

scaling factor is very likely to be different. In this section, we used the SSD scenarios described in Section 5.2 as an example to examine this estimation approach. To estimate the appropriate scaling factor  $\gamma^s$  for each city's SSD, we conduct simulations with the closed links across the entire simulation period. This allows us to generate the necessary information for the  $\gamma^s$ . Figure 6 demonstrates the average ratio of  $q(t)$  to  $D(t)$  from 10 simulation replications in different time intervals, excluding the warm-up and dissipation periods. Noteworthy, apart from the canceled trips originating from or heading to the closed area, there are also some trips cannot be carried on due to the absence of alternative routes, which are called interrupted trips here. Figure 6 presents two estimated  $\gamma^s$  values for each city: one considering all trips (in grey) and another one excluding interrupted trips (in red). For Munich, the former is smaller than  $\gamma$  while the latter is greater. In Kyoto, both are greater than  $\gamma$ . In general,  $\gamma^s$  should be greater than  $\gamma$  due to the network length decline and the trip length increase (because of detouring). However, this is not necessarily always true. If a large amount of long-distance trips were canceled for no available route alternatives, it is also possible to observe a decrease in the average trip length. In this case, the decrease proportions of the average trip length and network length will determine whether  $\gamma^s$  is greater than  $\gamma$ . The smaller  $\gamma^s$  obtained in Munich indicates that the average trip length under SSD reduces with a proportion of reduction smaller than that of the total network length.

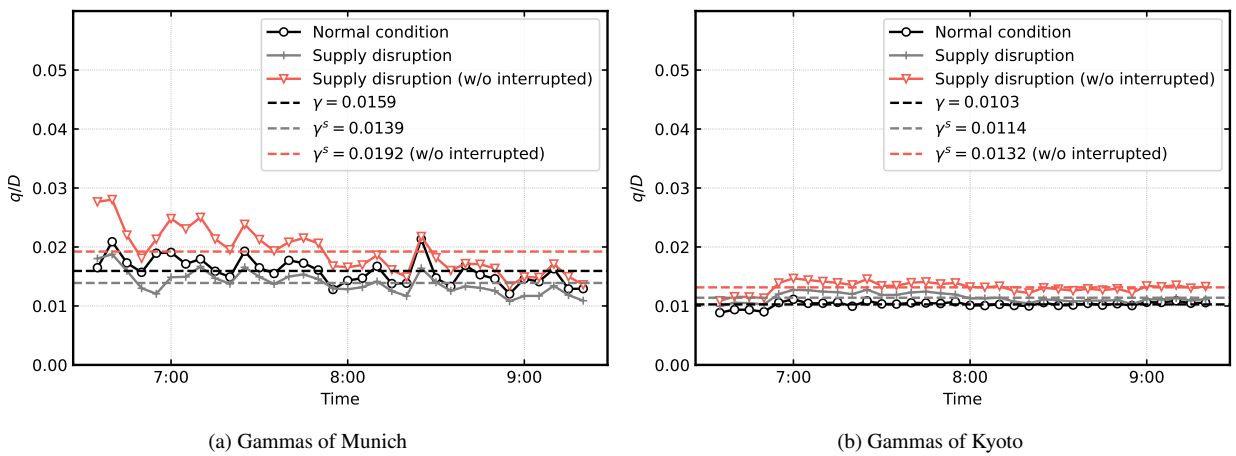


**Figure 6:** Estimation of  $\gamma$  under normal condition and supply disruption.

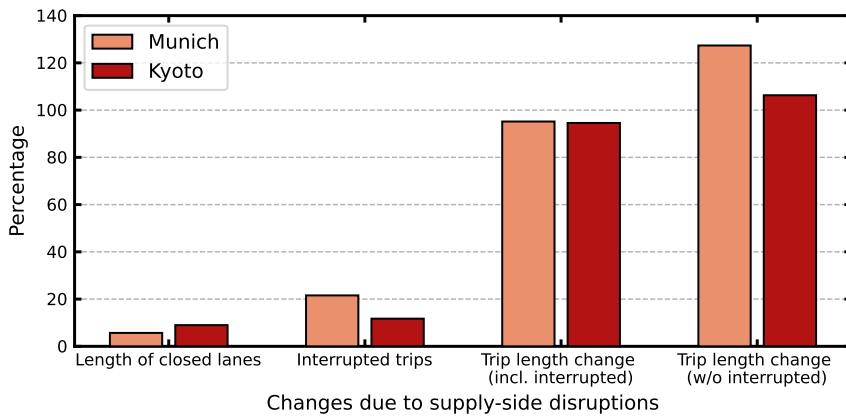


**Figure 7:** Changes in supply and demand due to supply-side disruptions

In order to explain the factors contributing to the difference, we also plot relevant trip statistics in Figure 7. As can be seen, approximately 12% of trips are interrupted in Kyoto, while this number increases to 21% in Munich. This disparity can be attributed to the grid structure of the Kyoto network, which provides more route alternatives between

every OD pair, enabling more trips to be rerouted after network disruption compared to the Munich network. This is also consistent with the finding in Zhang et al. (2015). Furthermore, the grid structure can also ease the vehicle detouring, represented by the minor average trip length increase. The average trip length of *completed* trips (i.e., trips reaching their destination) is 1.05 multiples of that under normal conditions in Kyoto, while this number is 1.27 in Munich. However, if we include the interrupted trips in the calculation, both cities reach a number of about 0.95, i.e., a reduction of about 5% in the average trip length. This value serves as a reference for the comparison of  $\gamma^s$  in the two cities. Figure 7 also depicts the percentage of the length of closed lanes in the complete network. Although we designed the scenarios by closing a similar proportion of links (7% for Kyoto and 8% for Munich), the total length of closed lanes comprises 8.98% (greater than 5%) and 5.68% (comparative to 5%) of the complete network of Kyoto and Munich, respectively. This leads to the difference of the change in  $\gamma^s$  between the two cities. It is worth mentioning that the errors between  $\gamma$ 's and  $L/L$  can be expressed by the estimation of the production using  $q$ . To eliminate the noise introduced by the interrupted trips, we improve the estimation by excluding those trips. The corrected values are also depicted in Figure 6 and will be utilized in the following evaluation.

Additionally, Figure 6 also illustrates that the traffic state in Munich is more stochastic than in Kyoto. This observation lends support to our assumption that different topology types (or cities) may exhibit varying relationship models between traffic resilience and network topological attributes, as discussed in Section 5.3. On the other hand, these findings also prove that distinguishing the influence of demand-side and supply-side factors is necessary for accurately modeling traffic resilience. Without clearly separating the consequence resulting from demand-side and supply-side factors will hinder the identification of the underlying stimuli for resilience loss, thereby leading to incorrect response actions.

## 6.2. MFD dynamics analysis under demand variations and infrastructure disruptions

Figure 8 shows the MFD dynamics (aggregated every 5 min) of the scenarios described in Section 5.2. In the case of Munich (Figure 8a), in terms of demand variations, we can see that neither scenario SD nor MD exceeds the critical point, indicating the absence of network-wide congestion. We can also see that the dynamics become more unstable as traffic approaches the critical point, which is consistent with the analysis in Gao et al. (2022). Furthermore, as shown in Figure 9a and 9b where results from different replications are averaged (with standard deviations shown), a clockwise hysteresis loop is observed in both scenarios, but the size of the hysteresis loop is almost doubled in MD compared to SD. The larger standard deviations observed in MD further confirm the presence of an unstable state around the critical point.

On the other hand, in scenario LD (Figure 9c), gridlock occurs in the network due to the over-saturated traffic. We find that the MFD dynamics are less dispersed in the vicinity of the critical point. Additionally, we plot the MFD dynamics for the scenario with supply disruption and large OD demand (LD-SSD) in Figure 8a. As expected and consistent with findings in Kim and Yeo (2017) and Gao et al. (2022), a noticeable reduction in weighted space-mean flow is found at the same accumulation level. However, the critical accumulation, in this case, denoted as  $n_c^s$ , is comparative to that of the normal system  $n_c$ . It indicates that using congestion deviation (i.e.,  $n(t) - n_c$ ) to model the resilience loss due to supply-side disruptions as in Gao et al. (2022) will lead to inaccurate estimation.

Figure 8b shows the traffic dynamics of Kyoto under different scenarios. Similar to the Munich case, Kyoto also experiences fluctuations in demand variation scenarios. In contrast, in terms of the LD-SSD, Kyoto almost suffers no degradation in the MFD shape. Therefore, it is unreasonable to directly use the area between the normal MFD curve and the disruptive MFD curve as the measurement of resilience loss as in Kim and Yeo (2017), as it will result in no or a very small resilience loss in Kyoto, which is incorrect as we showed in Section 6.3. Nevertheless, it is essential to note that differences do exist between the points of the same time interval under different scenarios, as explained in Section 3. This finding reaffirms the notion that the influencing mechanisms of congestion and supply-side disruptions are distinct, and therefore the traffic resilience to them should be discussed separately. It is thus reasonable to state that the resilience indicators proposed in this study are more reliable and robust for evaluating different types of disruptions and transportation systems.

## 6.3. Traffic resilience evaluation under demand variations and infrastructure disruptions

In this section, we evaluate and compare the traffic resilience of the Munich system and the Kyoto system. Two specific scenarios are considered for testing the system performance: Scenario LD is employed to assess the system's behavior under extreme demand situations, such as emergency travel demand, while scenario LD-SSD is utilized to test its performance in the presence of network or infrastructure malfunctions. For comparison purposes, we adopt

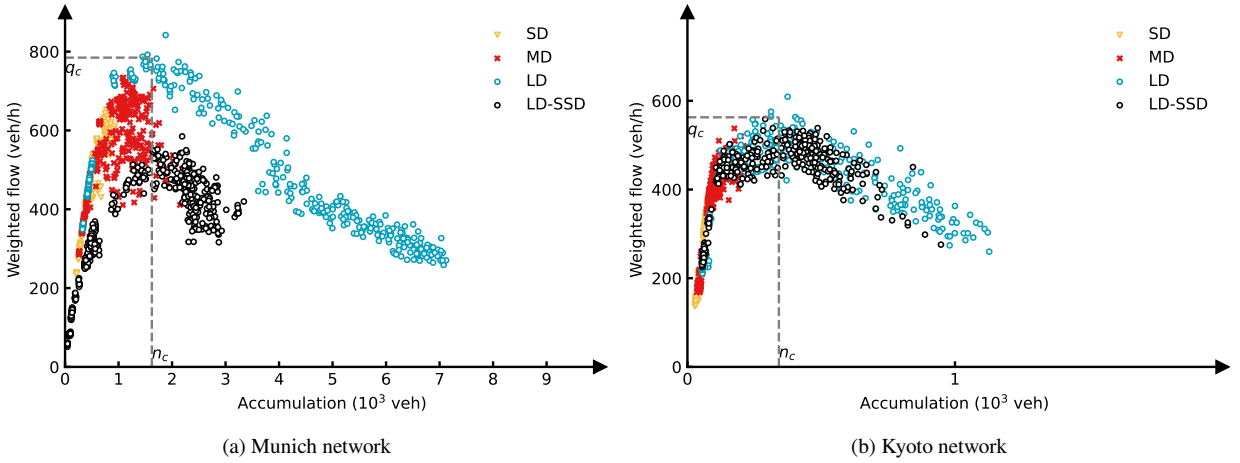


**Figure 8:** MFD dynamics of the scenarios of investigation.

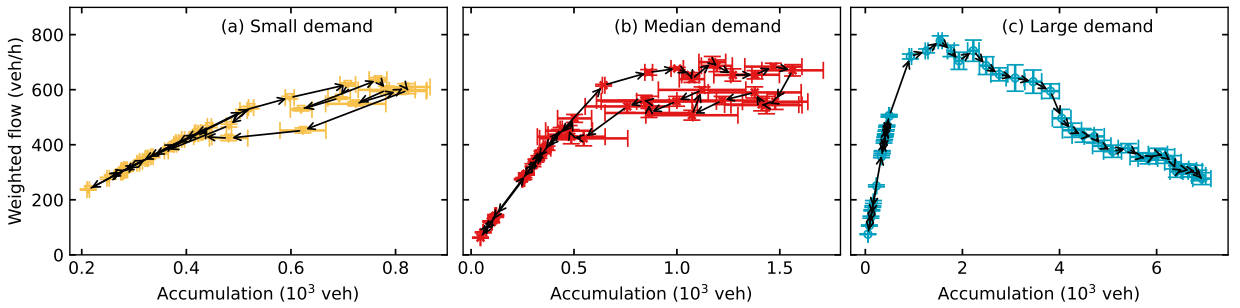


**Figure 9:** Development of MFD dynamics due to demand variations in Munich.

the formulation of normalized traffic resilience (i.e., Equations (16) and (17)) for the evaluation. The estimated  $\gamma$ 's presented in Section 6.1 are used for the normalization. The resilience loss curves (i.e., the normalized trip completion rate reduction over different time intervals) for congestion and supply-side disruptions in Munich are given in Figure 10a and 10b, respectively. The corresponding curves for Kyoto are given in Figure 10c and 10d.

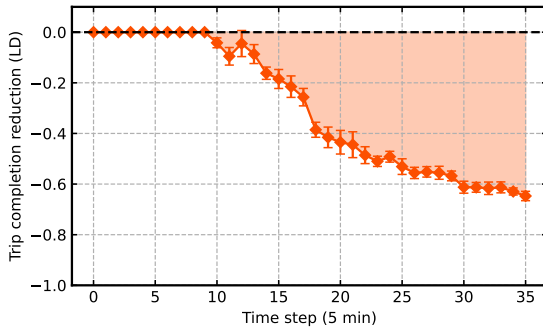
We note that the complete life cycle of the influence of congestion is not present due to the limitation of simulation duration (due to lack of demand data). The recovery process is missing in the LD experiments, which prevents us from drawing definitive conclusions regarding which city is more resilient to demand variations, especially when observing similar reduction speeds during the disruption phase in both cities.

On the contrary, from the curves for supply-side disruptions, it is evident that Kyoto is more resilient to supply-side disruptions (here, partial link closure), represented by a smaller area enclosed by the “resilience triangle”. The normalized traffic resilience losses,  $\tilde{R}^s$ , are -0.38 and -0.25 for Munich and Kyoto, respectively. As per the “4R” resilience properties (i.e., robustness, redundancy, resourcefulness, and rapidity) proposed in Bruneau et al. (2003) and characterized in Wan et al. (2018), we can draw the following conclusions: (i) A greater minimum value obtained in Kyoto represents stronger robustness in dealing with disruptions. (ii) A longer during-disruption duration (including response and recovery phases) in Kyoto implies that Munich outperforms Kyoto in terms of the property of rapidity. (iii) The resourcefulness property affects the shape of the system functionality curve during disruption. These two cities differ significantly from each other in this regard. To be specific, Munich gradually recovers after reaching the worst performance point, whereas Kyoto oscillates back and forth around that point until links are reopened. However, it is worth noting that the worst point in Kyoto is much better than in Munich, indicating that even during the disruption period, a stable “new equilibrium” can easily form in Kyoto. Nonetheless, future works on developing a specific quantitative measurement for the resourcefulness property would still be desirable. (iv) Due to the lack of a specific definition

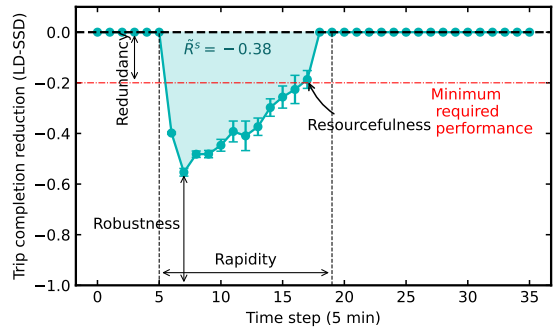
of “minimum required performance” here, redundancy cannot be specified. If a minimum required performance is defined as the example we provide in Figure 10b and 10d, i.e., -0.2 for each, the redundancy can be measured by its absolute value. However, the redundancy property can also be evaluated by the existence of optional routes for OD pairs. In this regard, grid-like networks usually outperform other kinds of networks. It is essential to consider these various resilience properties while evaluating the performance of transportation networks under different disruptions, as they provide valuable insight into how cities respond to and recover from disturbances.

Given that the network queue can be regarded as a part of traffic resilience loss under supply disruptions, the trends observed in the network queue curves presented in Figure 11 mirror those of the functionality curves illustrated in Figure 10. For comparison purposes, the network queues have also been normalized by the respective critical traffic flows  $q_c$ . While Munich exhibits a significantly longer network queue compared to Kyoto, it is noteworthy that the Kyoto system requires more time to clear the network queue.

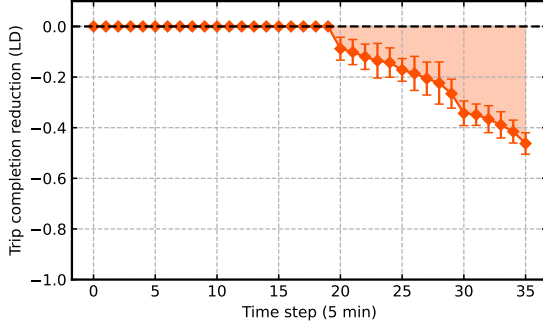
The analysis presented above clearly highlights the crucial role of network topology for traffic resilience. However, it is important to acknowledge that traffic resilience is not solely determined by network topological attributes; it is also significantly influenced by traffic dynamics, as evidenced by the earlier analysis. Therefore, the question of how much network topological attributes can account for traffic resilience necessitates further investigation and exploration.



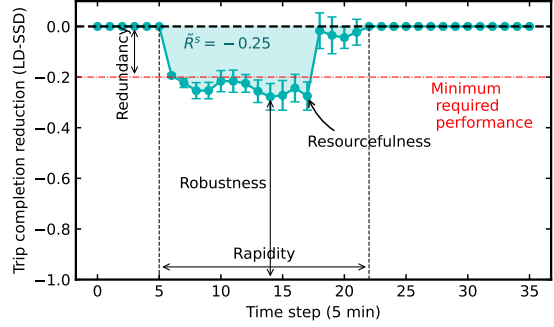
(a) Munich: Congestion



(b) Munich: Supply-side disruptions



(c) Kyoto: Congestion



(d) Kyoto: Supply-side disruptions

**Figure 10:** Traffic resilience under congestion and supply disruptions (large demand scenario).

#### 6.4. Comparison of MFD-based traffic resilience indicators

In Section 2.3, we analyzed the limitations of previous MFD-based resilience indicators and highlighted the advantages of our proposed indicators. To validate our analysis, we compare the curves of these normalized resilience indices under the LD-SSD scenario of Munich in Figure 12. We omit the indicator proposed by Kim and Yeo (2017) as it is static and cannot provide a comparative analysis. This also indicates that their establishment does not stem from the system functionality curve used in the system resilience definition.

Upon comparison, we observe that our index and Amini’s index (Amini et al., 2018) show a very close pattern during the disruption period. Amini’s index estimates slightly larger resilience loss during the disruption as its for-

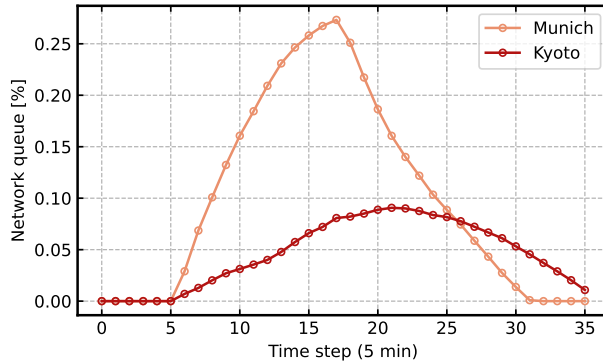


**Figure 11:** Network queue due to supply disruption (LD-SSD).

mulation neglects the reduction in network roadway length. Conversely, after the disruption, our index indicates the system recovers to the normal state, while Amini’s index counts the process of serving the vehicles delayed by the disruption as an increase in resilience. In terms of Gao’s index (Gao et al., 2022), no resilience loss is observed in the first 20 min of the disruption period. This can be attributed to the fact that, as highlighted in Section 2.3, this

5 indicator was proposed for hyper-congestion, and cannot identify the resilience loss caused by supply-side disruptions. Consequently, their index, known as congestion deviation, fails to capture the degradation in traffic states accurately, leading to an incorrect estimation of traffic resilience loss during the disruption period. Afterward, Gao’s index begins to decrease as a result of the rising number of vehicles in the network, where the accumulation surpasses its critical value. This index experiences a rebound of approximately 50% after the disruption as the system restores to its normal  
10 state and the critical accumulation also increases to its original value. It declines once more thereafter since the accumulation keeps increasing until the end of the investigation period. To provide a clearer presentation of the differences among these indices, Figure 12 does not display the entire curve of Gao’s index. Its value steadily decreases in the invisible region.

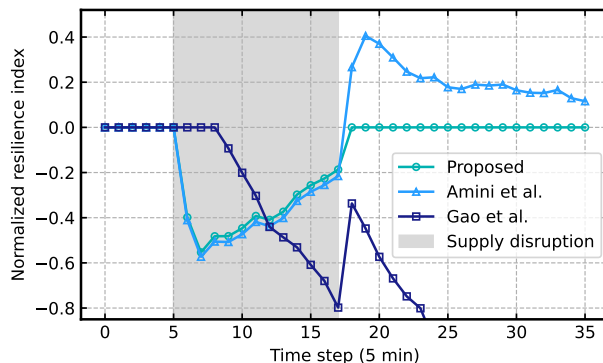


**Figure 12:** Comparison of MFD-based dynamic traffic resilience indicators (Munich LD-SSD scenario).

## 6.5. Relationship between topological attributes and traffic resilience

In this section, we conduct a regression analysis to understand the relationship between traffic resilience and network topology. The method described in Section 5.3 are used to create synthetic scenarios to generate required inputs, including topological variables as the explanatory dataset and resilience loss as the dependent variable. More specifically, the topological metrics listed in Table 2 of the network of each synthetic scenario are computed using the NetworkX (Hagberg et al., 2008) and OSMnx (Boeing, 2017) Python packages. The normalized resilience loss is estimated using the approach introduced in Section 3.6 based on the corresponding traffic dynamics generated from  
20

SUMO. The lasso model described in Section 4 is adopted for the regression analysis, given its sparse output that can help identify the most significant topological attributes. A  $\rho$  value of 0.001 is used for the lasso model.

### 6.5.1. Explanatory analysis of selected variables

We found that variables describing the same topological attribute/property are most highly correlated. To address multicollinearity, we removed variables with a correlation coefficient exceeding 0.7 from the explanatory dataset, resulting in the retention of four variables: degree assortativity, load centrality, average edge length, and Beta index. Finally, the lasso model results in non-zero coefficients for the degree assortativity, load centrality, and Beta index for both cities, while the coefficient for average edge length is zero. Since the p-value for degree assortativity is very large (0.935 for Munich and 0.883 for Kyoto), indicating little significance, we also removed it from the final regression model.

Figure 13 shows the value of the remaining variables identified and the dependent variable under different  $p$  values. Notably, each  $p$  value is associated with 100 scenarios, allowing us to construct boxplots that illustrate the distribution of variables. Different characteristics in load centrality can be observed between the two cities. Specifically, load centrality in Kyoto hovers around 0 across different  $p$  values but decreases with the increase of  $p$  in Munich. Load centrality in Munich almost remains the same when  $p \leq 0.08$ , suggesting that local centrality might only be impacted significantly after a sufficient number of links are closed, a phenomenon that may also be present in Kyoto. On the contrary, the Beta index is distributed similarly in the two cities and has similar change patterns.

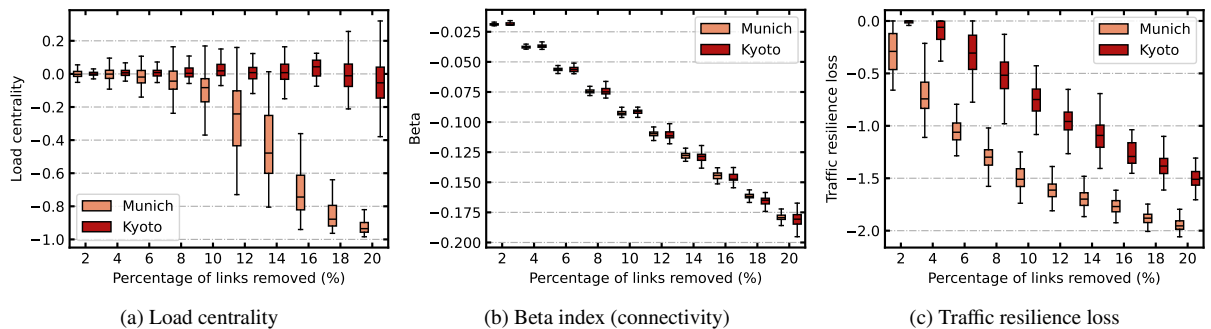


**Figure 13:** Boxplots for the selected explanatory variables and the dependent variable.

### 6.5.2. Regression model interpretation

Table 3 presents the model estimation results by solving the problem expressed by Equation (20). Only the variables with little correlations are inputted into the model, within which average edge length and degree assortativity are insignificant in both models, so it is not listed in the table. These two regression models reveal that significant topological attributes for traffic resilience are shared among different types of network topology. However, the significance levels and the extent to which they can explain traffic resilience are distinct.

**Table 3**

Regression model estimation

Variable	Topology Attr.	Coef. [p-value] (Kyoto)	Coef. [p-value] (Munich)
Load centrality	Centrality	-0.1016 [0.25]	-0.9778 [<0.0001]
Beta index	Connectivity	8.1062 [<0.0001]	16.6719 [<0.0001]
<b>Kyoto model</b>		<b>Munich model</b>	
# of samples: 925		# of samples: 949	
R-squared: 0.8583		R-squared: 0.7894	

Recall that all explanatory variables have been transformed to be the percentage reduction compared to the complete network using Equation (19). No intercepts are estimated considering the sense of physical interpretation. Conse-

quently, the coefficient of each specific variable reflects the sensitivity of traffic resilience to that variable. For instance, in the Kyoto model, a 10% reduction in the Beta index for three hours (the effective simulation duration) will lead to a loss of traffic resilience of about 0.81. According to the definition and interpretation of (normalized) traffic resilience provided in Section 3.5, it means that such a disruptive event can result in a cumulative service rate impairment of 81%. The larger absolute value of the coefficient for the Beta index in Munich suggests that Munich may experience more significant impairment than Kyoto when subjected to the same level of network connectivity reduction. This conclusion is also evident from Figure 13c, which demonstrates that with the same percentage of link removal, Munich exhibits a higher absolute traffic resilience loss compared to Kyoto. Furthermore, the relatively smaller coefficients for the other variables indicate that the Beta index is the most correlated and influential variable in our case studies. In other words, network connectivity plays a critical role in determining the traffic resilience of a transportation network. Conversely, the coefficient for load centrality in the regression models indicates that network centrality has a negative effect on traffic resilience. It means that urban planning should avoid increasing network centrality to enhance the network's traffic resilience to supply-side disruptions, which aligns with the findings from Wang et al. (2023) which found the negative relationship between node betweenness centrality and system resilience.

Further, referring back to Figure 13c, when the link removal probability  $p$  is small ( $\leq 0.04$ ), the deviation of resilience loss in Munich is considerably larger than that in Kyoto. It implies that random link removal may cause more uncertainty in the traffic states in Munich under non-serious disruptions. This observation is further supported by the much greater  $R^2$  obtained in the Kyoto model than in the Munich model. Therefore, it is fair to say that grid-like networks are more resilient and stable under supply-side disruptions in regard to traffic states. The good performance in  $R^2$  validates that the proposed traffic resilience indicator based on MFD dynamics not only can represent traffic dynamics but also capture the network structure characteristics. This can also be seen from the high correlation between the Beta index and traffic resilience.

## 7. Conclusions

This study investigated the problem of evaluating the traffic resilience of urban road transportation systems in a comprehensive and accurate manner. Traditional approaches have relied on static topology-based indicators, such as accessibility, or simple aggregation of trip information, such as average speed. However, these indicators have limitations: the former fails to capture the dynamic nature of traffic, while the latter is sensitive to travel demand. Moreover, both approaches do not adhere to the definition of system resilience as they cannot be considered inherent properties of networks. Recently, several indicators based on the concept of macroscopic fundamental diagrams (MFD) have been developed to measure the resilience of urban transportation systems from multiple perspectives. Unlike other resilience indicators, MFD-based indicators possess the advantage of being network properties, as MFD represents an intrinsic characteristic of a homogeneously congested network. Nonetheless, existing MFD-based indicators have certain drawbacks, such as insufficient consideration of network structure changes, neglecting the detouring or rerouting of vehicles, or relying on inaccurate reference points.

To overcome the aforementioned limitations, this study introduces a novel approach that offers a comprehensive evaluation of traffic resilience of urban road transportation systems. Our approach specifically addresses the distinct influencing mechanisms of congestion and supply-side disruptions. Notably, while supply-side disruptions may alter the shape of the MFD, traffic congestion does not have the same effect. Starting with the consideration that the functionality of a system/facility is usually represented by its service rate, the trip completion rate of the entire network is used as the base of evaluation. Then, we separately discussed traffic resilience to congestion and supply-side disruptions and built the respective indicators accordingly. Additionally, we outline a methodology for discretizing and normalizing the calculation of traffic resilience loss, enabling practical applications and facilitating comparative analyses. By using the proposed indicators, traffic resilience loss can be physically interpreted as the cumulative number of vehicles that should have finished their trips within the respective time intervals if the transportation system/network were operating optimally under normal conditions (without infrastructure malfunction). Moreover, we devote attention to the relationship between topological attributes and traffic resilience. To this end, we propose a synthetic supply-side disruption scenario generation procedure, which can be used to generate a diverse set of observations as input for a regularized linear regression model. This allows for the examination of various topological attributes and their impact on traffic resilience.

We conducted experiments in two distinct cities — Munich, Germany, and Kyoto, Japan, which possess different network topologies. The experimental results provided evidence for the superiority of our proposed approach and indi-

cators over previous MFD-based indicators in terms of reliability and robustness. Furthermore, our findings revealed that Kyoto's grid-like network demonstrates greater resilience to supply-side disruptions compared to Munich's central ring structure. Several factors contribute to this disparity: (i) Grid-like networks offer more route alternatives between every OD pair so that more trips can be rerouted after network disruption; (ii) The grid structure can also ease the vehicle detouring. Our regression models for the two cities indicated that significant topological attributes influencing traffic resilience are generally consistent across different network topologies. However, the extent to which these attributes explain traffic resilience differs. Notably, we found that network connectivity, measured by the Beta index in this study, emerged as the most correlated and significant attribute of traffic resilience. A larger coefficient value for the Beta index in Munich suggests that Munich may experience a more pronounced service rate impairment than Kyoto when confronted with a similar reduction in network connectivity. This finding aligns with the conclusion that grid-like networks are more resilient than central ring networks, as supported by previous literature (e.g., [Zhang et al., 2015](#)). The high correlation between traffic resilience and topological attributes proved that the proposed indicator based on MFD dynamics not only can represent traffic dynamics but also capture the network structure characteristics.

We suggest the following directions for future research:

- We acknowledge the potential occurrence of mixed scenarios resulting from the interplay between a supply-side disruption and emergency demand (attributed to recovery actions or public panic), as discussed in Section 3.4. However, the analysis of related scenarios in the experiment results is limited. Future studies can be undertaken to develop a reliable approach to design plausible mixed disruption scenarios and explore the interaction and interdependence between traffic resilience of these two types of disruptions.
- To further enhance our understanding of the relationship between traffic resilience and network topology, future research endeavors can explore additional types of network topology. While this study primarily focused on two specific types of topology due to data constraints, it is important to acknowledge that the insights gained in this regard are inherently limited. To overcome this limitation, one potential approach is to create synthetic networks representing various types of network topology using advanced traffic simulation techniques. A key challenge in synthetic network generation lies in creating reasonable OD demand matrices for comparative analysis. This paper's findings suggest that a network's traffic resilience can be explained by its topological attributes to a certain extent. Therefore, integrating these attributes with other relevant information, such as network size and population data, could potentially serve as a surrogate for traffic resilience. The prospect of deriving a general relationship model from experimental results across numerous network scenarios is promising. Such a model could facilitate the evaluation of the transportation networks of real cities and assist in the design of resilient transportation networks in a simple manner.
- As revealed in Section 2.1, resilience indicators typically serve as a component of the objective function in the optimization problems related to pre-disruption mitigation/preparedness and post-disruption recovery strategies. Thus, traffic resilience-oriented optimization and control will be another promising avenue for future research. By utilizing the MFD-based traffic resilience indicators proposed in this study, one can identify effective strategies without the need for detailed traffic dynamics information across the entire network. One of our ongoing work is to develop simulation-based traffic resilience optimization models that account for different preparedness and recovery measures. The distinction between evaluating congestion and supply-side disruptions enables the identification of the most efficient and suitable response measures for each type of disruption. In practice, the MFD under normal conditions can be established by utilizing observed traffic data, which is a one-time step unless significant changes in demand patterns. Subsequently, the simulation model can be calibrated with the MFD as the objective. As such, once the network experiences a disruption, the potential disruptive traffic state can be estimated or the disruptive MFD can be calibrated correspondingly. Optimization models can then be applied to tackle the problem. However, the proposed indicators are non-smooth, restricting the application of numerous solution algorithms. Therefore, any smooth approximations would be beneficial.

## Acknowledgements

This research was supported by the CONCERT-Japan DARUMA project (Grant Number: 01DR21010) funded by the German Federal Ministry of Education and Research (BMBF), Germany, and by JST SICORP Grant Number JPMJSC20C4, Japan. This research was also partially funded by the DAAD-Kyoto University Partnership Programme (Grant Number: 57664680).

## Appendix A Mesoscopic simulation model calibration

For the calibration of the mesoscopic simulation model, we mainly focus on the OD matrices calibration by using the traffic counts collected by loop detectors. Normalized root mean square error (RMSN) is used to evaluate the performance of calibration, which is given by

$$\text{RMSN} = \frac{\sqrt{N \sum_{i=1}^N (\hat{y}_i - y_i)^2}}{\sum_{i=1}^N y_i} \quad (21)$$

where  $y_i$  and  $\hat{y}_i$  are the observed and simulated traffic counts at detecting location  $i$ ,  $N$  denotes the total number of detecting locations.

For the Kyoto model, we use the movement matrices of *Docomo* (a Japanese mobile phone operator) users as the initial guess of the vehicle mobility patterns. Considering the difference in the scales of the two groups, we first find out the scaling factors resulting in the smallest RMSN for each time interval by simply trying different convex combinations of predefined lower and upper bounds. This step improves the matrices from an RMSN error of 1.2 to 0.74. It indicates that the mobility patterns of mobile phone users can resemble that of vehicles to a certain extent. We note that the study area is only a part of the city of Kyoto, and only partial links of the Kyoto network are included. As a result, the amount of through traffic is very different from the ones extracted from mobile phone data (Lu et al., 2023) due to : (i) All vehicles can only use the network provided to finish their trips which is inconsistent with reality in which some can reach their destinations by the paths outside this network; (ii) Vehicles from the area outside the study area have not been counted. To address this issue, we first apply the simultaneous perturbation stochastic approximation (SPSA) algorithm (Spall, 1998) to correct the OD demand from/to the outermost zones to additionally measure the demand from/to external zones. Utilizing the corrected OD matrix as the prior, we then employ the PC-SPSA algorithm (Qurashi et al., 2022) to calibrate the whole OD matrix. Finally, the average RMSN reduces to a satisfactory level of 0.41.

For the Munich model, the reader is referred to the authors' previous studies in Lu et al. (2021) and Dadashzadeh et al. (2021) for more details about its calibration.

## References

- Ahmed, M.A., Sadri, A.M., Mehrabi, A., Azizinamini, A., 2022. Identifying topological credentials of physical infrastructure components to enhance transportation network resilience: case of florida bridges. Journal of transportation engineering, Part A: Systems 148, 04022055.
- Amghar, R., Jaber, S., Moghaddam, S.H.M., Bhouri, N., Ameli, M., 2024. Resilience as a service for transportation networks: Definition and basic concepts. Transportation Research Record 2678, 177–189.
- Amini, K., Padgett, J.E., 2023. Probabilistic risk assessment of hurricane-induced debris impacts on coastal transportation infrastructure. Reliability Engineering & System Safety 240, 109579.
- Amini, S., Tilg, G., Busch, F., 2018. Evaluating the impact of real-time traffic control measures on the resilience of urban road networks, in: 2018 21st International Conference on Intelligent Transportation Systems (ITSC), pp. 519–524.
- Anderson, M., Kiddle, D., Logan, T., 2022. The underestimated role of the transportation network: Improving disaster & community resilience. Transportation research part D: transport and environment 106, 103218.
- Aparicio, J.T., Arsenio, E., Henriques, R., 2022. Assessing robustness in multimodal transportation systems: a case study in lisbon. European transport research review 14, 1–18.
- Arango, E., Nogal, M., Yang, M., Sousa, H.S., Stewart, M.G., Matos, J.C., 2023. Dynamic thresholds for the resilience assessment of road traffic networks to wildfires. Reliability Engineering & System Safety , 109407.
- Balal, E., Valdez, G., Miramontes, J., Cheu, R.L., 2019. Comparative evaluation of measures for urban highway network resilience due to traffic incidents. International Journal of Transportation Science and Technology 8, 304–317.
- Boeing, G., 2017. Osmnx: New methods for acquiring, constructing, analyzing, and visualizing complex street networks. Computers, Environment and Urban Systems 65, 126–139.
- Bruneau, M., Chang, S.E., Eguchi, R.T., Lee, G.C., O'Rourke, T.D., Reinhorn, A.M., Shinozuka, M., Tierney, K., Wallace, W.A., Von Winterfeldt, D., 2003. A framework to quantitatively assess and enhance the seismic resilience of communities. Earthquake spectra 19, 733–752.
- Bucar, R.C., Hayeri, Y.M., 2020. Quantitative assessment of the impacts of disruptive precipitation on surface transportation. Reliability Engineering & System Safety 203, 107105.
- Byun, J.E., D'Ayala, D., 2022. Urban seismic resilience mapping: a transportation network in istanbul, turkey. Scientific reports 12, 8188.
- Chacon-Hurtado, D., Kumar, I., Gkritza, K., Fricker, J.D., Beaulieu, L.J., 2020. The role of transportation accessibility in regional economic resilience. Journal of Transport Geography 84, 102695.
- Chalkiadakis, C., Perdikouris, A., Vlahogianni, E.I., 2022. Urban road network resilience metrics and their relationship: Some experimental findings. Case Studies on Transport Policy 10, 2377–2392.

- Chen, C., Huang, Y., Lam, W., Pan, T., Hsu, S., Sumalee, A., Zhong, R., 2022. Data efficient reinforcement learning and adaptive optimal perimeter control of network traffic dynamics. *Transportation Research Part C: Emerging Technologies* 142, 103759.
- Chen, C., Wang, S., Zhang, J., Gu, X., 2023. Modeling the vulnerability and resilience of interdependent transportation networks under multiple disruptions. *Journal of Infrastructure Systems* 29, 04022043.
- 5 Chen, L., Miller-Hooks, E., 2012. Resilience: An indicator of recovery capability in intermodal freight transport. *Transportation Science* 46, 109–123.
- Dadashzadeh, N., Elvarsson, A.B., Morshed, G., Agresti, S.A., Antoniou, C., Roncoli, C., Thomopoulos, N., 2021. Autonomous and connected transport scenarios evaluation based on simulation analysis: Wg5: Thematic report .
- Diab, E., Shalaby, A., 2020. Metro transit system resilience: Understanding the impacts of outdoor tracks and weather conditions on metro system 10 interruptions. *International Journal of Sustainable Transportation* 14, 657–670.
- Dingil, A.E., Rupi, F., Stasiskiene, Z., 2019. A Macroscopic analysis of transport networks: The influence of network design on urban transportation performance. *International Journal of Transport Development and Integration* 3, 331–343.
- Dong, S., Gao, X., Mostafavi, A., Gao, J., Gangwal, U., 2023. Characterizing resilience of flood-disrupted dynamic transportation network through 15 the lens of link reliability and stability. *Reliability Engineering & System Safety* 232, 109071.
- Fang, C., Chu, Y., Fu, H., Fang, Y., 2022. On the resilience assessment of complementary transportation networks under natural hazards. *Transportation research part D: transport and environment* 109, 103331.
- FHWA, 2015. Transportation system resilience to extreme weather and climate change. <https://ops.fhwa.dot.gov/publications/fhwahop15025/fhwahop15025.pdf> (Last accessed on 2023-06-20).
- Ganin, A.A., Mersky, A.C., Jin, A.S., Kitsak, M., Keisler, J.M., Linkov, I., 2019. Resilience in Intelligent Transportation Systems (ITS). *Transportation Research Part C: Emerging Technologies* 100, 318–329.
- Gao, J., Barzel, B., Barabási, A.L., 2016. Universal resilience patterns in complex networks. *Nature* 530, 307–312.
- Gao, S., Li, D., Zheng, N., Hu, R., She, Z., 2022. Resilient perimeter control for hyper-congested two-region networks with MFD dynamics. *Transportation Research Part B: Methodological* 156, 50–75.
- Geroliminis, N., Daganzo, C.F., 2008. Existence of urban-scale macroscopic fundamental diagrams: Some experimental findings. *Transportation Research Part B: Methodological* 42, 759–770.
- Guidotti, R., Gardoni, P., Chen, Y., 2017. Network reliability analysis with link and nodal weights and auxiliary nodes. *Structural Safety* 65, 12–26.
- Hagberg, A.A., Schult, D.A., Swart, P.J., 2008. Exploring network structure, dynamics, and function using networkx, in: Varoquaux, G., Vaught, T., Millman, J. (Eds.), *Proceedings of the 7th Python in Science Conference*, Pasadena, CA USA. pp. 11 – 15.
- Hao, Y., Jia, L., Zio, E., Wang, Y., Small, M., Li, M., 2023. Improving resilience of high-speed train by optimizing repair strategies. *Reliability Engineering & System Safety* 237, 109381.
- Hoogendoorn, S.P., Knoop, V.L., van Lint, H., Vu, H.L., 2015. Applications of the Generalized Macroscopic Fundamental Diagram, in: Chraibi, M., Boltes, M., Schadschneider, A., Seyfried, A. (Eds.), *Traffic and Granular Flow'13*. Springer International Publishing, pp. 577–583.
- Huang, J., Levinson, D.M., 2015. Circuitry in urban transit networks. *Journal of Transport Geography* 48, 145–153.
- Huang, Y., Xiong, J., Sumalee, A., Zheng, N., Lam, W., He, Z., Zhong, R., 2020. A dynamic user equilibrium model for multi-region macroscopic 35 fundamental diagram systems with time-varying delays. *Transportation Research Part B: Methodological* 131, 1–25.
- Jana, D., Malama, S., Narasimhan, S., Taciroglu, E., 2023. Edge-based graph neural network for ranking critical road segments in a network. *Plos one* 18, e0296045.
- Kim, S., Yeo, H., 2017. Evaluating link criticality of road network based on the concept of macroscopic fundamental diagram. *Transportmetrica A: Transport Science* 13, 162–193.
- 40 Kurth, M., Kozlowski, W., Ganin, A., Mersky, A., Leung, B., Dykes, J., Kitsak, M., Linkov, I., 2020. Lack of resilience in transportation networks: Economic implications. *Transportation Research Part D: Transport and Environment* 86, 102419.
- Levinson, D., 2012. Network structure and city size. *PLoS One* 7, e29721.
- Liu, T., Bai, G., Tao, J., Zhang, Y.A., Fang, Y., 2024. A multistate network approach for resilience analysis of uav swarm considering information exchange capacity. *Reliability Engineering & System Safety* 241, 109606.
- 45 Liu, T., Bai, G., Tao, J., Zhang, Y.A., Fang, Y., Xu, B., 2022. Modeling and evaluation method for resilience analysis of multi-state networks. *Reliability Engineering & System Safety* 226, 108663.
- Lopez, P.A., Behrisch, M., Bieker-Walz, L., Erdmann, J., Flötteröd, Y.P., Hilbrich, R., Lücken, L., Rummel, J., Wagner, P., Wießner, E., 2018. Microscopic traffic simulation using sumo, in: 2018 21st international conference on intelligent transportation systems (ITSC), IEEE. pp. 2575–2582.
- 50 Lu, Q.L., Qurashi, M., Antoniou, C., 2023. Simulation-based policy analysis: The case of urban speed limits. *Transportation Research Part A: Policy and Practice* 175, 103754.
- Lu, Q.L., Qurashi, M., Varesanovic, D., Sodnik, J., Antoniou, C., 2021. Exploring the influence of automated driving styles on network efficiency. *Transportation research procedia* 52, 380–387.
- Miller-Hooks, E., Zhang, X., Faturechi, R., 2012. Measuring and maximizing resilience of freight transportation networks. *Computers & Operations Research* 39, 1633–1643.
- Mirjalili, R., Barati, H., Yazici, A., 2023. Resilience analysis of new york city transportation network after snow storms. *Transportation research record* 2677, 694–707.
- Narayanan, S., Antoniou, C., 2022. Electric cargo cycles-a comprehensive review. *Transport policy* 116, 278–303.
- Pan, S., Yan, H., He, J., He, Z., 2021. Vulnerability and resilience of transportation systems: A recent literature review. *Physica A: Statistical 60 Mechanics and its Applications* 581.
- Parthasarathi, P., 2014. Network structure and metropolitan mobility. *Journal of transport and land use* 7, 153–170.
- Pei, S., Zhai, C., Hu, J., 2024. Surrogate model-assisted seismic resilience assessment of the interdependent transportation and healthcare system considering a two-stage recovery strategy. *Reliability Engineering & System Safety* 244, 109941.

- Qurashi, M., Lu, Q.L., Cantelmo, G., Antoniou, C., 2022. Dynamic demand estimation on large scale networks using principal component analysis: The case of non-existent or irrelevant historical estimates. *Transportation Research Part C: Emerging Technologies* 136, 103504.
- Roy, K.C., Cebrian, M., Hasan, S., 2019. Quantifying human mobility resilience to extreme events using geo-located social media data. *EPJ Data Science* 8, 1–15.
- Safitri, N.D., Chikaraishi, M., 2022. Impact of transport network disruption on travel demand: A case study of the july 2018 heavy rain disaster in japan. *Asian Transport Studies* 8, 100057.
- Santiago-Iglesias, E., Carpio-Pinedo, J., Sun, W., García-Palomares, J.C., 2023. Frozen city: Analysing the disruption and resilience of urban activities during a heavy snowfall event using google popular times. *Urban Climate* 51, 101644.
- Serdar, M.Z., Koç, M., Al-Ghamdi, S.G., 2022. Urban transportation networks resilience: indicators, disturbances, and assessment methods. *Sustainable Cities and Society* 76, 103452.
- Shekar, V., Fiondella, L., Chatterjee, S., Halappanavar, M., 2017. Quantitative assessment of transportation network vulnerability with dynamic traffic simulation methods, in: 2017 IEEE International Symposium on Technologies for Homeland Security (HST), IEEE. pp. 1–7.
- Somy, S., Shafeai, R., Ramezanian, R., 2022. Resilience-based mathematical model to restore disrupted road-bridge transportation networks. *Structure and Infrastructure Engineering* 18, 1334–1349.
- Spall, J.C., 1998. Implementation of the simultaneous perturbation algorithm for stochastic optimization. *IEEE Transactions on Aerospace and Electronic Systems* 34, 817–823.
- Su, Z., Chow, A.H., Zheng, N., Huang, Y., Liang, E., Zhong, R., 2020. Neuro-dynamic programming for optimal control of macroscopic fundamental diagram systems. *Transportation Research Part C: Emerging Technologies* 116, 102628.
- Taghizadeh, M., Mahsuli, M., Poorzahedy, H., 2023. Probabilistic framework for evaluating the seismic resilience of transportation systems during emergency medical response. *Reliability Engineering & System Safety* 236, 109255.
- Virtucio, M.B., Cetiner, B., Zhao, B., Soga, K., Taciroglu, E., 2024. A granular framework for modeling the capacity loss and recovery of regional transportation networks under seismic hazards: A case study on the port of los angeles. *International Journal of Disaster Risk Reduction* 100, 104164.
- Wan, C., Yang, Z., Zhang, D., Yan, X., Fan, S., 2018. Resilience in transportation systems: A systematic review and future directions. *Transport Reviews* 38, 479–498.
- Wang, N., Wu, M., Yuen, K.F., 2023. A novel method to assess urban multimodal transportation system resilience considering passenger demand and infrastructure supply. *Reliability Engineering & System Safety* 238, 109478.
- Wassmer, J., Merz, B., Marwan, N., 2024. Resilience of transportation infrastructure networks to road failures. *Chaos: An Interdisciplinary Journal of Nonlinear Science* 34.
- Wei, D., Rose, A., Koc, E., Chen, Z., Soibelman, L., 2022. Socioeconomic impacts of resilience to seaport and highway transportation network disruption. *Transportation Research Part D: Transport and Environment* 106, 103236.
- Wu, Y., Chen, S., 2023. Traffic resilience modeling for post-earthquake emergency medical response and planning considering disrupted infrastructure and dislocated residents. *International Journal of Disaster Risk Reduction* 93, 103754.
- Xu, Z., Chopra, S.S., 2022. Network-based assessment of metro infrastructure with a spatial-temporal resilience cycle framework. *Reliability Engineering & System Safety* 223, 108434.
- Yang, Z., Barroca, B., Weppe, A., Bony-Dandrieux, A., Laffréchine, K., Daclin, N., November, V., Omrane, K., Kamissoko, D., Benaben, F., et al., 2023. Indicator-based resilience assessment for critical infrastructures—a review. *Safety Science* 160, 106049.
- Yao, K., Chen, S., 2023. Percolation-Based Resilience Modeling and Active Intervention of Disrupted Urban Traffic Network during a Snowstorm. *Journal of Transportation Engineering, Part A: Systems* 149, 04023027.
- Yin, J., Ren, X., Liu, R., Tang, T., Su, S., 2022. Quantitative analysis for resilience-based urban rail systems: A hybrid knowledge-based and data-driven approach. *Reliability Engineering & System Safety* 219, 108183.
- Yin, K., Wu, J., Wang, W., Lee, D.H., Wei, Y., 2023. An integrated resilience assessment model of urban transportation network: A case study of 40 cities in china. *Transportation Research Part A: Policy and Practice* 173, 103687.
- Zeng, G., Li, D., Guo, S., Gao, L., Gao, Z., Stanley, H.E., Havlin, S., 2019. Switch between critical percolation modes in city traffic dynamics. *Proceedings of the National Academy of Sciences* 116, 23–28.
- Zhang, M., Yang, X., Zhang, J., Li, G., 2022a. Post-earthquake resilience optimization of a rural “road-bridge” transportation network system. *Reliability Engineering & System Safety* 225, 108570.
- Zhang, N., Alipour, A., 2023. A stochastic programming approach to enhance the resilience of infrastructure under weather-related risk. *Computer-Aided Civil and Infrastructure Engineering* 38, 411–432.
- Zhang, W., Dong, H., Wen, J., Han, Q., 2023a. A resilience-based decision framework for post-earthquake restoration of bridge networks under uncertainty. *Structure and Infrastructure Engineering*, 1–16.
- Zhang, X., Miller-Hooks, E., Denny, K., 2015. Assessing the role of network topology in transportation network resilience. *Journal of Transport Geography* 46, 35–45.
- Zhang, Y., Zheng, S., Chen, Y., 2023b. Identification of key nodes in comprehensive transportation network: A case study in beijing-tianjin-hebei urban agglomeration, china. *Transportation Research Record*, 03611981231192994.
- Zhang, Z., Ji, T., Wei, H.H., 2022b. Dynamic emergency inspection routing and restoration scheduling to enhance the post-earthquake resilience of a highway–bridge network. *Reliability Engineering & System Safety* 220, 108282.
- Zhang, Z., Ji, T., Wei, H.H., 2023c. Assessment of post-earthquake resilience of highway–bridge networks by considering downtime due to interaction of parallel restoration actions. *Structure and Infrastructure Engineering* 19, 589–605.
- Zhong, R., Chen, C., Huang, Y., Sumalee, A., Lam, W., Xu, D., 2018. Robust perimeter control for two urban regions with macroscopic fundamental diagrams: A control-lyapunov function approach. *Transportation Research Part B: Methodological* 117, 687–707.